

# Rain-on-snow responses to a warmer Pyrenees: a sensitivity analysis using a physically-based hydrological model

Josep Bonsoms<sup>1</sup>, Juan I. López-Moreno<sup>2</sup>, Esteban Alonso-González<sup>3</sup>, César Deschamps-Berger<sup>2</sup>, Marc Oliva<sup>1</sup>

<sup>1</sup> Department of Geography, Universitat de Barcelona, Barcelona, Spain

<sup>2</sup> Instituto Pirenaico de Ecología (IPE-CSIC), Campus de Aula Dei, Zaragoza, Spain

<sup>3</sup> Centre d'Etudes Spatiales de la Biosphère (CESBIO), Université de Toulouse, CNES/CNRS/IRD/UPS, Toulouse, France.

Corresponding author: Juan I. López-Moreno (nlopez@ipe.csic.es)

**Abstract.** Climate warming is changing the magnitude, timing, and spatial patterns of mountain snowpacks. A warmer atmosphere may also lead to precipitation phase shifts, with decreased snowfall fraction (Sf). The combination of Sf and snowpack decreases directly affects the frequency and intensity of rain-on-snow (ROS) events, a common cause of flash-flood events in snow dominated regions. In this work we examine the ROS patterns and sensitivity to temperature and precipitation change in the Pyrenees modelling through a physical-based snow model forced with reanalysis climate data perturbed using a range of values of temperature and precipitation consistent with 21<sup>st</sup> century climate projections. ROS patterns are characterized by their frequency, rainfall quantity and snow ablation. The highest ROS frequency for the historical climate period (1980 – 2019) are found in South-West high-elevations sectors of the Pyrenees (17 days/year). Maximum ROS rainfall amount is detected in South-East mid-elevations areas (45 mm/day, autumn), whereas the highest ROS ablation is found in North-West high-elevations zones (- 10 cm/day, summer). When air temperature is increased from 1°C to 4°C with respect to the historical climate period, ROS rainfall amount and frequency increase at a constant rate during winter and early spring for all elevation zones. For the rest of the seasons, non-linear responses of the ROS frequency and ablation to warming are found. Overall, ROS frequency decreases in the shoulders of the season across eastern low-elevated zones due to snow cover depletion. However, ROS increases in cold, high-elevated zones where long-lasting snow cover exists until late spring. Similarly, warming induces greater ROS ablation (+ 10% per °C) during the coldest months of the season, high-elevations, and northern sectors where the deepest snow depths are found. On the contrary, small differences in ROS ablation are found for warm and marginal snowpacks. These results highlight the different ROS responses to warming across the mountain range, suggest similar ROS sensitivities in near mid-latitude zones, and will help anticipate future ROS impacts in hydrological, environmental, and socioeconomic mountain systems.

**Keywords:** Snow, Rain-on-snow, Climate warming, Snow sensitivity, Mountain snowpack, Pyrenees.

## 26 **1 Introduction**

27

28 Mountain snowpacks supply large hydrological resources to the lowlands (García-Ruiz et al., 2015; Viviroli et  
29 al., 2011), with important implications in the ecological (Wipf and Rixen, 2010), hydrological (Barnett, 2005;  
30 Immerzeel et al., 2020) and socioeconomic systems by providing hydroelectricity (Beniston et al., 2018) or  
31 guaranteeing winter tourism activities (Spandre et al., 2019). Climate warming, however, is modifying  
32 mountain snowfall patterns (IPCC, 2022), through temperature-induced precipitation changes from snowfall  
33 to rainfall (Lynn et al., 2020), leading in some cases to rain-on-snow (ROS) events in snow covered areas  
34 where it did not occur before. The upward high-latitude temperature and precipitation trends (Bintanja and  
35 Andry, 2017) and warming in mountain regions (Pepin et al., 2022) will likely change future ROS frequency  
36 in snow-dominated areas (López-Moreno et al., 2021). ROS has relevant impacts in the ecosystem. The liquid  
37 water percolation in the snowpack due to a ROS event creates ice layers and could alter its stability (Rennert  
38 et al., 2009). In severe ROS events, water percolation reaches the ground, and the subsequent water freezing  
39 causes latent heat releases, leading to soil and permafrost warming (Westermann et al., 2011). Positive heat  
40 fluxes during ROS events enhance snow runoff (Corripio and López-Moreno, 2017), especially in warm and  
41 wet snowpacks (Würzer et al., 2016). ROS can also trigger a snow avalanche in mountain zones (Conway and  
42 Raymond, 1993), flash flood events (Surfleet and Tullos, 2013), impacts in tundra ecosystems (Hansen et al.,  
43 2014) and herbivore populations (Kohler and Aanes, 2004).

44 Different ROS frequency trends have been found since the last half of the 20<sup>st</sup> century. In the western United-  
45 States and from 1949 to 2003 (McCabe et al., 2007) found a general ROS frequency decrease in 1500 m but an  
46 increase in high elevations. Similarly, the analysis of six major German basins from 1990 to 2011, reveals an  
47 upward (downward) ROS frequency trend during winter (spring) at 1500 m and high elevations (Freudiger et  
48 al., 2014). On the contrary, from 1979 to 2014, no winter ROS frequency trends were found across the entire  
49 Northern-Hemisphere (Cohen et al., 2015). ROS projections for the end of the 21<sup>st</sup> century suggest a general  
50 ROS frequency increase in cold regions and high elevated zones (IPCC, 2019). This is projected for Alaska  
51 (Bieniek et al., 2018), Norway (Mooney and Li, 2021), western United-States (Musselman et al., 2018),  
52 Canada (il Jeong and Sushama, 2018) or Japan (Ohba and Kawase, 2020). In European mid-latitude mountain  
53 ranges, such as the Alps, ROS frequency is expected to increase (decrease) in high (low) elevation sectors  
54 (Beniston and Stoffel, 2016; Morán-Tejeda et al., 2016). López-Moreno et al. (2021) compared the ROS  
55 sensitivity to climate warming across 40 global basins and detected the highest ROS frequency decreases in  
56 low-elevated and warm Mediterranean mountain sites. Despite the increasing understanding of ROS spatio-  
57 temporal past and future trends, little is known about the ROS sensitivity to climate warming across southern  
58 European mountain ranges, such as the Pyrenees.

59

60 Here we examine the ROS sensitivity to temperature and precipitation change for low (1500 m), mid (1800 m)  
61 and high (2400 m) elevations of the Pyrenees. ROS responses to temperature and precipitation is analyzed  
62 using a physically based snow model, forced with reanalysis climate data (1980 – 2019) perturbed according  
63 to a range of temperature and precipitation changes consistent with 21<sup>st</sup> century climate projections for the

64 mountain range (Amblar-Francés et al., 2020). Previous studies in alpine zones have shown different ROS  
65 response to warming depending on the area and month of the season (e.g., Morán-Tejeda et al. 2016). For this  
66 reason, results are focused on these two factors. First, we analyze height of snow (HS) and snowfall fraction  
67 (Sf) responses to temperature and precipitation since these are the main variables that control ROS events  
68 (López-Moreno et al., 2021). Next, we examine ROS patterns and their response to warming by three key ROS  
69 indicators, namely:

70

71 (a) Number of ROS days for a season (ROS frequency).

72 (b) Average rainfall quantity during a ROS day (ROS rainfall amount).

73 (c) Average daily snow ablation during a ROS day (ROS ablation).

74

75 The study area is presented in Section 2. Section 3 describes the data and methods. Section 4 presents the  
76 results. We finally discuss the anticipated ROS spatio-temporal changes, their socio-environmental impacts  
77 and hazards in Section 5.

78

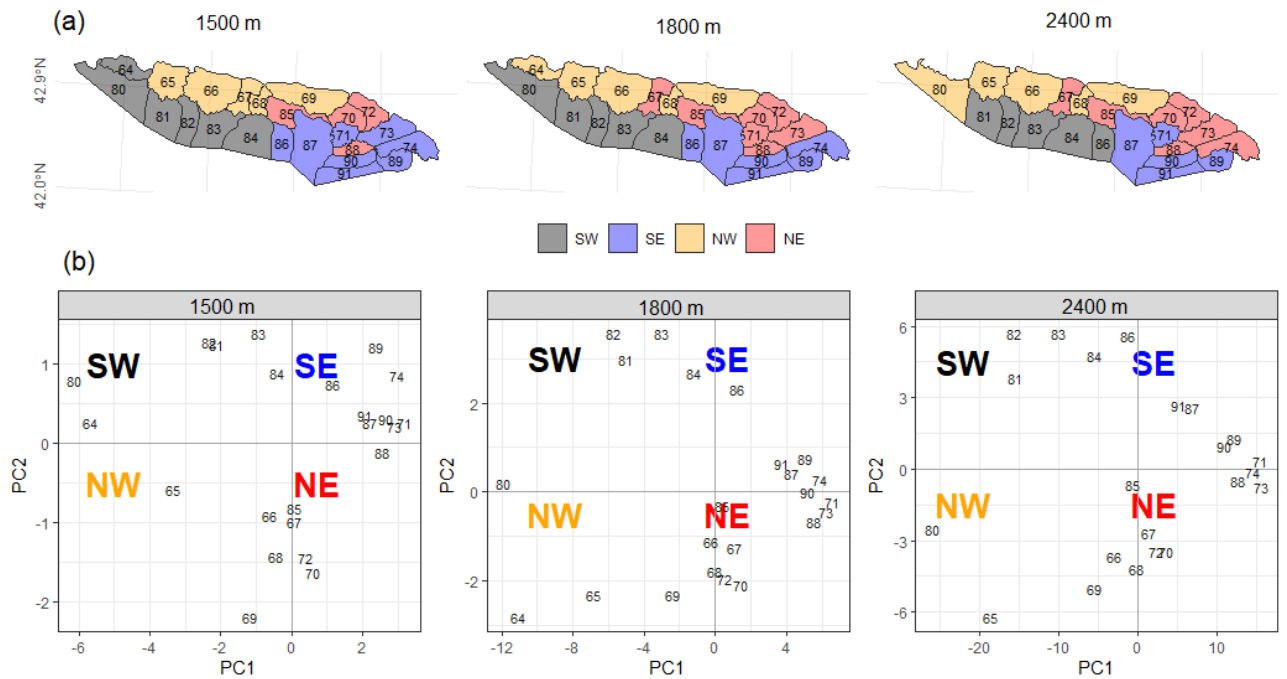
## 79 **2 Regional setting**

80

81 The Pyrenees Mountain range is located between the Atlantic Ocean (West) and the Mediterranean Sea (East)  
82 and is the largest (~ 450 km) mountain range of the Iberian Peninsula. Elevation increases towards the central  
83 massifs, where the highest peak is found (Aneto, 3,404 m asl). Glaciers expanded during the Little Ice Age and  
84 nowadays are in the highest mountain summits (Vidaller et al., 2021). The regional annual 0 °C isotherm is at  
85 ca. 2700 m (Del Barrio et al., 1990), and at ca. 1600 m during the cold season (López-Moreno and Vicente-  
86 Serrano, 2011). The elevation lapse-rate is ca. 0.6°/100 m, being slightly lower during winter (Navarro-Serrano  
87 and López-Moreno, 2017). Annual precipitation is ca. 1000 mm/year (ca. 1500 m); maximum values are found  
88 in the northern-western massifs (around 2000 mm/year), decreasing towards the southern-eastern (SE) area  
89 (Lemus-Canovas et al., 2019). Precipitation is predominantly (> 90%) solid above 1600 m from November to  
90 May (López-Moreno, 2005). Due to the mountain alignment, relief configuration, and the distance to the  
91 Atlantic Ocean, seasonal snow accumulations in the northern slopes (ca. 500 cm/season), almost doubles the  
92 recorded in the SE area for the same elevation (ca. 2000 m) (Bonsoms et al., 2021b). In the western and central  
93 area of the southern slopes of the range (SW sector, Figure 1), snow accumulation is ruled by Atlantic wet and  
94 mild flows, which are linked with negative North Atlantic Oscillation (NAO) phases (SW and W synoptic  
95 weather types) (López-Moreno, 2005; Alonso-González et al., 2020b; Bonsoms et al., 2021a). Positive Western  
96 Mediterranean Oscillation (WeMO) phases (NW and NE synoptic weather types) control the snow patterns in  
97 the northern-eastern (NE) slopes of the range (Bonsoms et al., 2021a). Generally, snow ablation starts in  
98 February at low elevations and in May at high elevation. The energy available for snow ablation is controlled  
99 by net radiation (55 %, over the total), latent (32 %) and sensible (13 %) heat fluxes (Bonsoms et al., 2022).

100

101



103

104

105

106

107

108

109

110

111

112

113

114

115

116

117

118

119

120

121

122

123

124

125

126

**Figure 1.** (a) Pyrenean massifs sectors (colors) for 1500 m, 1800 m and 2400 m elevation. Massifs were classified according to a Principal Component Analysis (PCA) applied over monthly HS data of each massif and elevation range for all months and years of the historical climate period (1980 – 2019). (b) PCA scores of each massif for 1500 m, 1800 m and 2400 m elevation. The black numbers are the SAFRAN massif's identity numbers defined by Vernay et al. (2022). Note that 2400 m elevation does not include massif number 64 since this massif does not reach that elevation range..

### 3 Data and methods

#### 3.1 Snow model description

The snowpack is simulated using the energy and mass balance snow model FSM2 (Essery, 2015). The FSM2 was forced at hourly resolution for each massif and elevation range (c.f. Sect. 3.3) for the historical climate period (1980 – 2019) and perturbed using a range of values of temperature and precipitation changes consistent with 21<sup>st</sup> century climate projections (c.f. Sect. 3.4). Sf was quantified using a threshold-approach. Precipitation was snowfall when temperature was < 1 °C according to previous ROS research in the study zone (Corripio and López-Moreno, 2017) and the average rain-snow temperature threshold for the Pyrenees (Jennings et al., 2018). Snow cover fraction is calculated by a linear function of snow depth, snow albedo is estimated based on a prognostic function with the new snowfall. Snow thermal conductivity is estimated based on snow density. Liquid water percolation is calculated based on a gravitational drainage. Compaction rate is simulated from overburden and thermal metamorphism. The atmospheric stability is estimated through the Richardson number stability functions to simulate latent and sensible heat fluxes. The selected FSM2 configuration includes three snow layers and four soil layers. The FSM2 configuration selected is shown in

Table S1. The FSM2 model and configuration was previously validated in the Pyrenees at Bonsoms et al. (2023). FSM2 has been successfully used in snow model sensitivity studies in alpine zones (Günther et al., 2019). FSM2 has been implemented in a wide range of alpine conditions, such as for the Iberian Peninsula mountains (Alonso-González et al., 2019), Spanish Sierra Nevada (Collados-Lara et al., 2020) or Swiss forest environments (Mazzotti et al., 2020) snowpack modeling. FMS2 has been integrated in snow data-assimilation schemes in combination with in-situ (Smyth et al., 2022) and remote-sensing data (Alonso-González et al., 2022).

134

### 3.2 Atmospheric forcing data

136

The FSM2 was forced with the SAFRAN meteorological system reanalysis dataset for flat terrain (Vernay et al., 2022). The SAFRAN meteorological system integrates meteorological simulations, remote-sensing cloud cover data, and instrumental records through data-assimilation. SAFRAN is forced with a combination of ERA-40 reanalysis (1958 to 2002) and the numerical weather prediction model ARPEGE (2002 to 2020). SAFRAN system was firstly designed for hazard forecasting (Durand et al., 1999, 2009)SAFRAN has been extensively validated as meteorological forcing data for the snow modeling in complex alpine terrain (Revuelto et al., 2018; Deschamps-Berger et al., 2022), to study long-term snow evolution (Réveillet et al., 2022), avalanche hazard forecasting (Morin et al., 2020), snow climate projections (Verfaillie et al., 2018), snow depth (López-Moreno et al., 2020) and energy heat fluxes spatio-temporal trends (Bonsoms et al., 2022).

146

### 3.3 Spatial areas

148

SAFRAN system provides data at hourly resolution from 0 to 3600 m, by steps of 300 m, grouped by massifs. The SAFRAN massifs (polygons of Figure 1) were chosen for their relative topographical and climatological similarities (Durand et al., 1999). We selected the 1500 m (low), 1800 m (mid), and 2400 m (high) specific elevation bands of the Pyrenees. In order to retain the main spatial differences across the mountain range, reduce data dimensionality and include the maximum variance, massifs with similar interannual snow characteristics were grouped into sectors by performing a Principal Component Analysis (PCA). PCA is an extensively applied statistical method for climatological and snow spatial regionalization (i.e., López-Moreno and Vicente-Serrano, 2007; Schöner et al., 2019; Alonso-González et al., 2020a; Matiu et al., 2021; Bonsoms et al., 2022). A PCA was applied over HS data for all months and years of the historical climate period. Massifs were grouped into four groups depending on the maximum correlation to the first (PC1) and second (PC2) scores. Pyrenean sectors were named South-West (SW), South-East (SE), North-West (NW) and North-East (NE) due to their geographical position. Figure 1 shows the resulting Pyrenean regionalization for 1500 m, 1800 m and 2400 m elevation as well as the SAFRAN massifs PC1 and PC2.

162

### 3.4 Sensitivity analysis

164

ROS season extension was defined according to ROS occurrence during the historical climate period. For the purposes of this research, seasons are classified as follows: October and November (Autumn); December, January, and February (Winter); March, April, May, and June (Spring); and July (Summer). August and September are not included due to the absence of regular snow cover. Sf, HS and ROS sensitivity to air temperature and precipitation is analyzed by perturbing climate data (López-Moreno et al., 2013; Pomeroy et al., 2015; Marty et al., 2017; Musselman et al., 2017b; Rasouli et al., 2019; Alonso-González et al., 2020a; López-Moreno et al., 2021). Specifically, SAFRAN reanalysis climate data was perturbed according to Spanish Meteorological Agency air temperature and precipitation projections for the 21st century in the Pyrenees (Amblar-Francés et al., 2020). Precipitation was increased (+10%), left unchanged (0 %) and decreased (-10%). Air temperature (°C) was perturbed between +1°C and +4°C by steps of +1°C. Incoming longwave radiation was increased due to warming, by applying the Stefan-Boltzmann law, using the Stefan-Boltzmann constant ( $\sigma$ ;  $5.670373 \times 10^{-8} \text{ W m}^{-2} \text{ K}^{-4}$ ), and the hourly atmospheric emissivity ( $\epsilon_t$ ) derived from SAFRAN air temperature and incoming longwave radiation:

178

179

180

$$\epsilon_t = \frac{LW_{in}}{\sigma(T_a + 273.15)^4}$$

Where  $T_a$  is air temperature and  $LW_{in}$  is incoming longwave radiation. An increase of air temperature of 1°C can be interpreted as a low emission scenario for the region, while 2°C and 4°C would represent projections for mid and high emission scenarios, respectively (Pons et al., 2015). The range of +/-10% for precipitation includes the expected changes in precipitation according to most climate models, regardless of the emission scenario (López-Moreno et al., 2008; Pons et al., 2015; Amblar-Francés et al., 2020).

186

### 187 3.5 ROS definition and indicators

188

The average HS and Sf sensitivity to temperature and precipitation (expressed in % per °C of local warming) is the average seasonal HS and Sf anomalies under the historical climate period and divided by degree of warming. Days are classified as ROS days when daily rainfall amount was  $\geq 10$  mm and HS  $\geq 0.1$  m, according to previous works (Musselman et al., 2018; López-Moreno et al., 2021). ROS frequency is the number of ROS days. ROS rainfall amount (mm/day) is the average daily rainfall (mm) during a ROS day. ROS ablation is the average daily snow ablation (cm/day) during a ROS day. The average daily snow ablation is the daily average HS difference between two consecutive days (Musselman et al., 2017a). Only the days when a negative HS difference occurred were selected.

197

## 198 4 Results

199

We provide an analysis of Sf, HS, and ROS patterns response to temperature and precipitation change. ROS spatio-temporal dynamics are analyzed in terms of frequency, rainfall quantity and snow ablation. Since we

202 have detected a non-linear ROS sensitivity to temperature, ROS indicators values are shown as a function of  
203 the change in temperature and precipitation amounts, grouped by elevation and sectors, namely SW, SE, NW  
204 and NE.

205

#### 206 **4.1 HS and Sf response to temperature and precipitation change**

207

208 HS and Sf response to temperature and precipitation is shown in Figure 2. Seasonal HS and Sf variability is  
209 mostly controlled by the increment of temperature, season, elevation, and spatial sector. The role of  
210 precipitation variability in the seasonal HS evolution is moderate to low (Figure S1 to S3). Only at 2400 m  
211 elevation an upward trend of precipitation (at least > 10%) can counterbalance small increments of temperature  
212 (< 1°C, over the historical climate period) from December to February (Figure S4). For this reason,  
213 precipitation was excluded to further analysis, and the ROS sensitivity analysis is evaluated for the average  
214 change of precipitation. Snow at 1500 m and 1800 m elevations during summer is rarely observed, however,  
215 marginal snow cover at 2400 m elevation can last until June and July, especially in the wettest sectors of the  
216 range (NW and SW). Seasonal HS and Sf response to temperature show large seasonality. The average HS  
217 reduction ranges from 39 %, 37 % and 28 % per °C, for 1500 m, 1800 m and 2400 m elevations, respectively.  
218 However, relevant differences are found depending on the season and degree of warming (Figure 3). Maximum  
219 HS and Sf reductions are found in 1500 m and 1800 m elevations during the shoulders of the season (autumn  
220 and spring). In these elevations, maximum HS decreases (52 % over the historical climate period) are simulated  
221 for spring when temperature is + 1°C. The greatest HS decreases in 2400 m elevation areas are simulated for  
222 summer (54 % HS decrease for 1°C). If temperature reaches maximum values (+ 4 °C), seasonal HS is reduced  
223 by 92 %, 89 %, and 79 % for 1500 m, 1800 m, and 2400 m elevations, respectively (Figure S4).

224

225

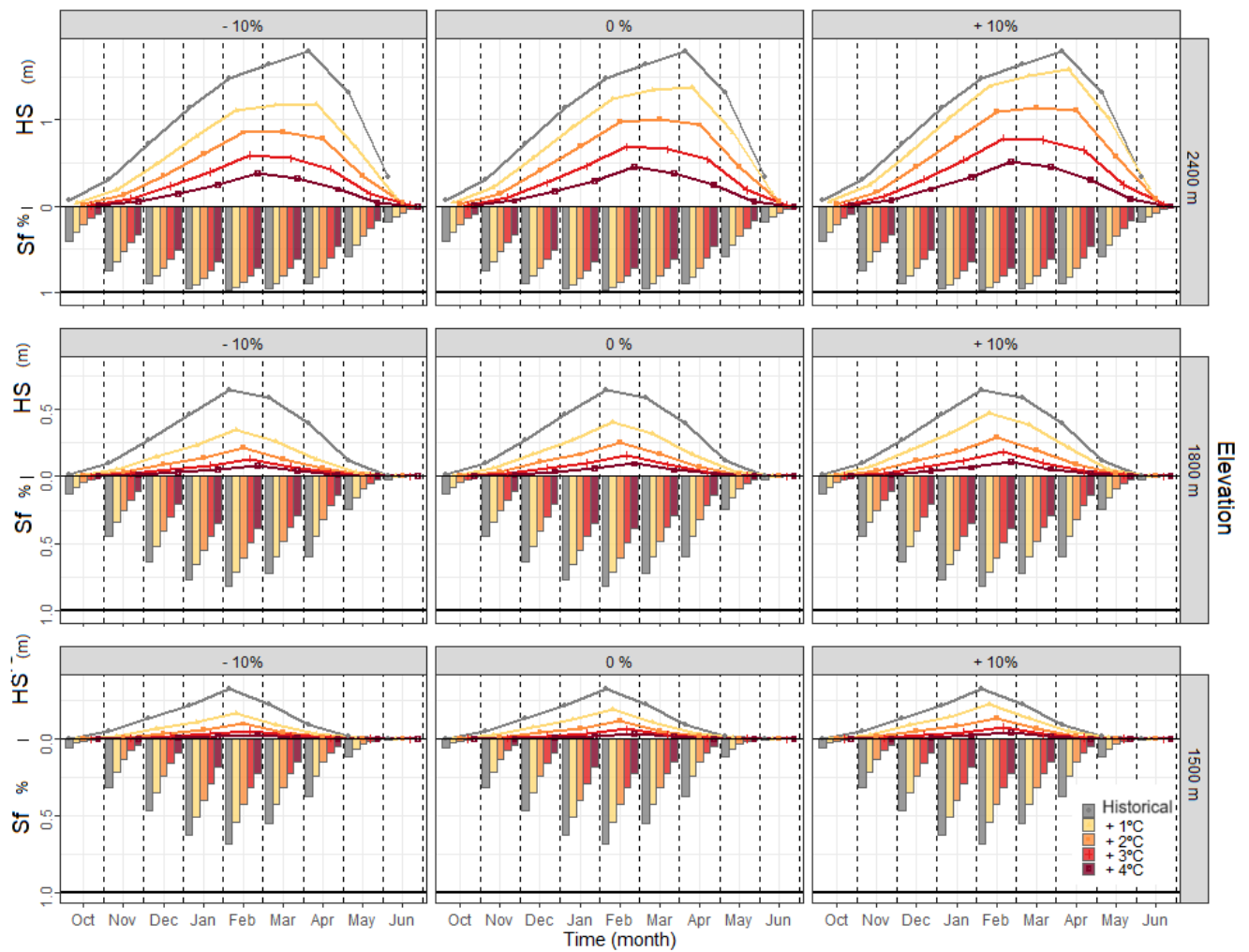


**Figure 2.** Height of snow (HS) (lines) and Snowfall fraction (Sf) (bars) monthly variation for the historical climate period (1980 – 2019) and different increments of temperature (colors) grouped by precipitation change and elevation (boxes). Note that Sf values (y-axis) are inverted.



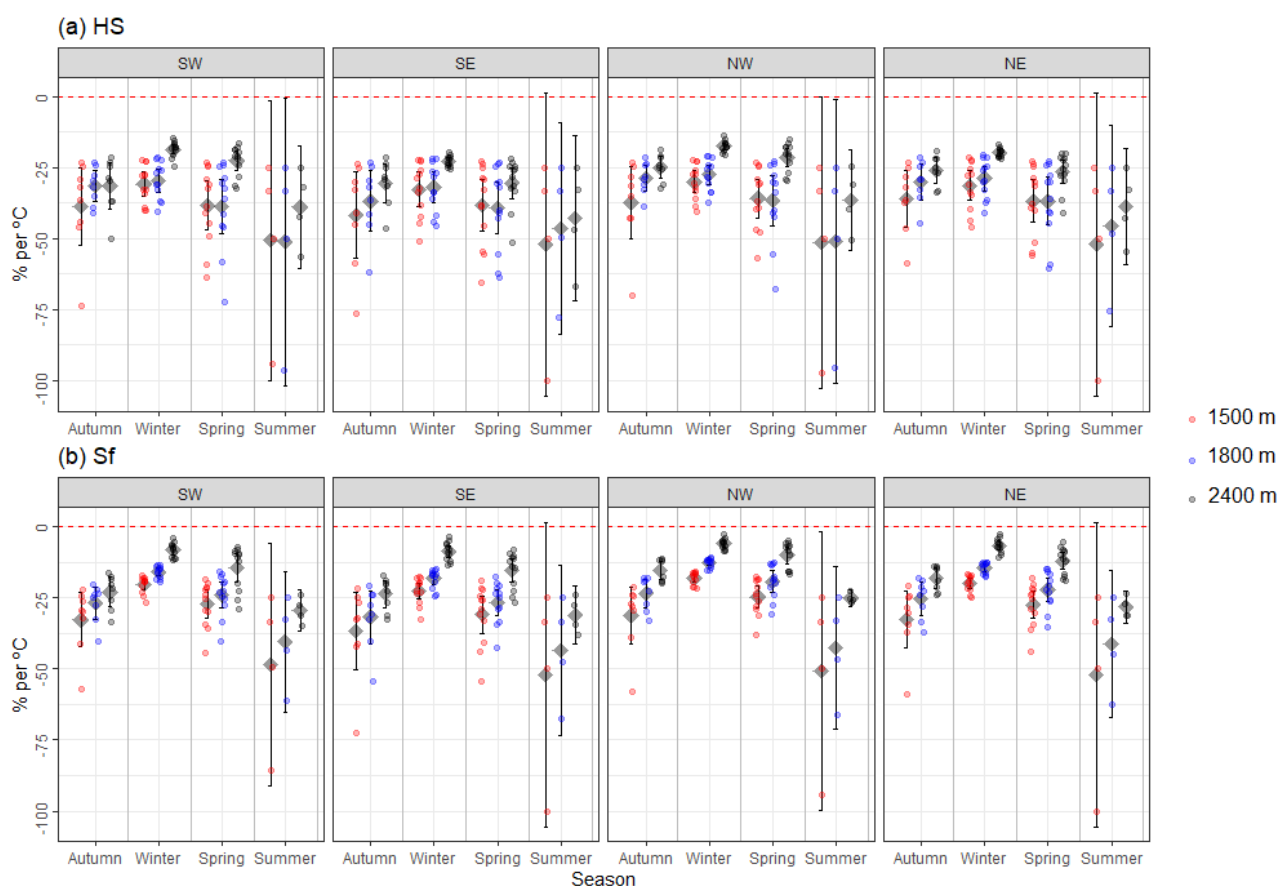
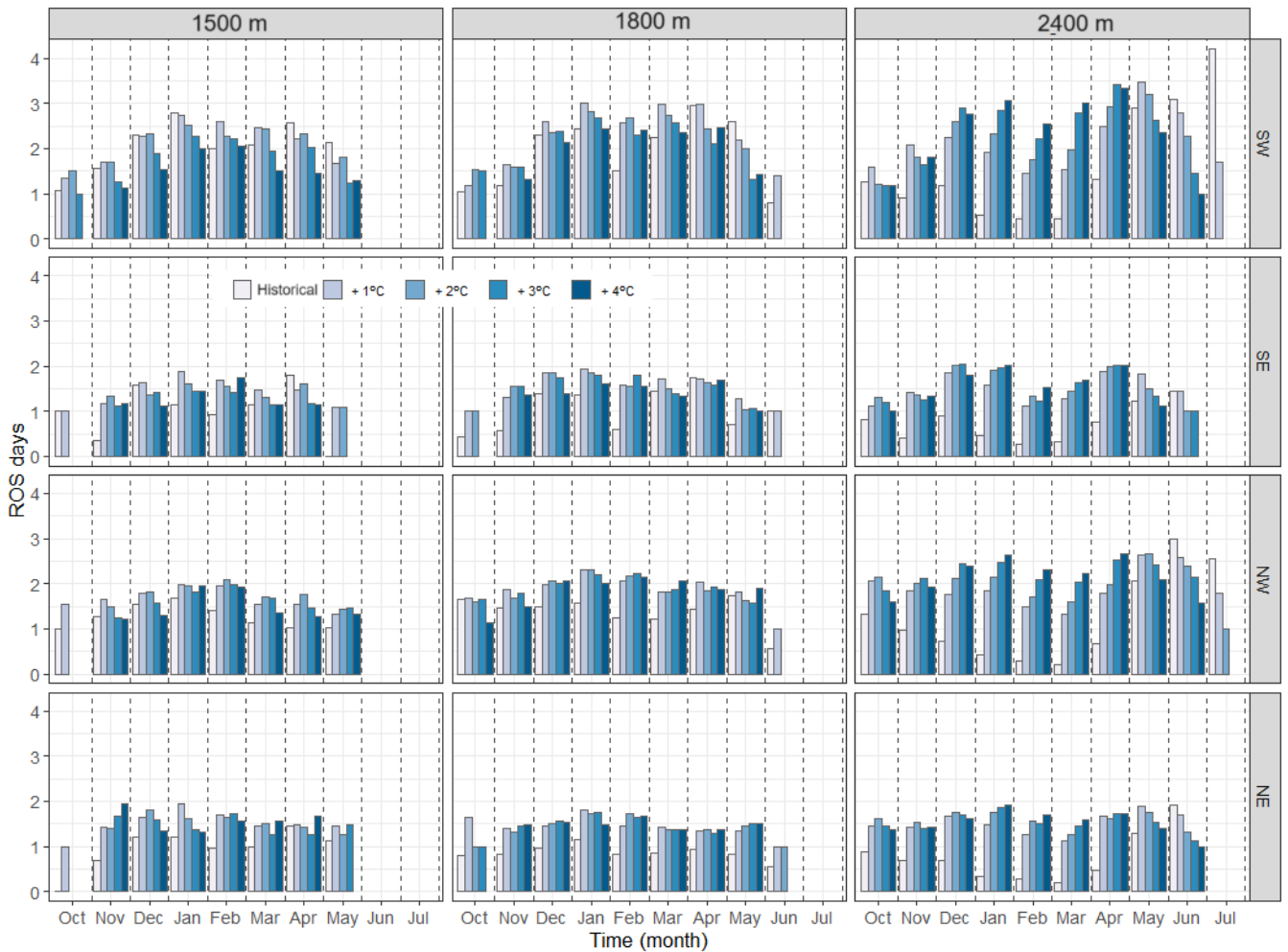


**Figure 3.** Seasonal (a) HS and (b) Sf anomalies over the historical climate period (1980 – 2019). Data are shown by elevation (colors), season (x-axis) and sectors (boxes). Points represent the average seasonal HS and Sf anomalies grouped by month of the season and increment of temperature (from 1°C to 4°C). The black diamond point indicates the mean, whereas the upper and lower error bars show the Gaussian confidence based on the normal distribution. Data are the average of the simulated precipitation change (from -10% to 10%, by steps of 10%).

## 4.2 ROS frequency

During the historical climate period (1980 – 2019), annual ROS frequency totals on average 10, 12 and 10 day/season for 1500 m, 1800 m and 2400 m elevations. However, there are large differences depending on the sector. 1500 m elevation annual ROS frequency for the historical climate period is 17, 8, 10 and 7 days/year for SW, SE, NW, NE sectors, respectively (Figure 4). The highest annual ROS frequency is however observed

253 at 1800 m elevation. Here, annual ROS frequency is 17, 9, 12 and 9 for SW, SE, NW, NE sectors. Within these  
 254 elevations, the maximum ROS frequency is detected in SW during winter and spring (7 days/season, for both  
 255 elevations and seasons). The eastern Pyrenees follow a similar seasonality. Maximum ROS frequency at 1500  
 256 m elevation is found in winter (4 and 3 days/season, SE and NE, respectively), and during spring at 1800 m  
 257 elevation (4 and 3 days, SE and NE, respectively). ROS is rarely observed in SE during the latest month of  
 258 spring (May), which contrast with the simulated values for SW (2 and 3 days/month, for 1500 m and 1800 m  
 259 elevations, respectively). 2400 m elevation shows the minimum ROS frequency. Here, comparisons between  
 260 seasons reveal maximum ROS frequency during summer, especially in SW (7 days/season), followed by NW  
 261 (6 days/season), and NE (2 days/season).



265  
 266  
 267 **Figure 4.** ROS frequency for the historical climate period (1980 – 2019) and increments of temperature  
 268 (colors), grouped by months (x-axis), sector (rows) and elevation (columns). Data are the average of the  
 269 simulated precipitation change (from -10% to 10%, by steps of 10%).  
 270  
 271 ROS frequency response to warming vary depending on the month, increment of temperature, elevation, and

272 sector. ROS tends to disappear in October for 1500 m elevation for + 1°C, except in SW (Figure 4 and 5). The  
273 highest increases are seen during the winter for increments temperature lower than 3°C, particularly in NE,  
274 where ROS frequency increases 1 day per month over the historical climate period for + 1°C. At 1800 m  
275 elevation, ROS frequency increases in all regions from November to February (around 1 day per month, for +  
276 1°C up to + 3°C). Similar increases are expected in NW and SW during the earliest months of spring and for  
277 1500 m to moderate increments of temperature. The contrary is observed during the latest months of spring in  
278 SW, where warming reduces ROS events. A slight ROS frequency increase is found during spring for the rest  
279 of the sectors (Figure 4). ROS events in June are expected to disappear for temperature increases higher than  
280 1°C. Finally, 2400 m elevation shows the largest ROS frequency variations (around 1 day/month for + 1°C).  
281 Maximum ROS frequency increases (3 days/month) are found in SW for more than + 3°C. ROS frequency  
282 progressively increases in March and April for all sectors but tends to decrease in May (for + 3°C), June and  
283 July (for + 1°C).

284

285

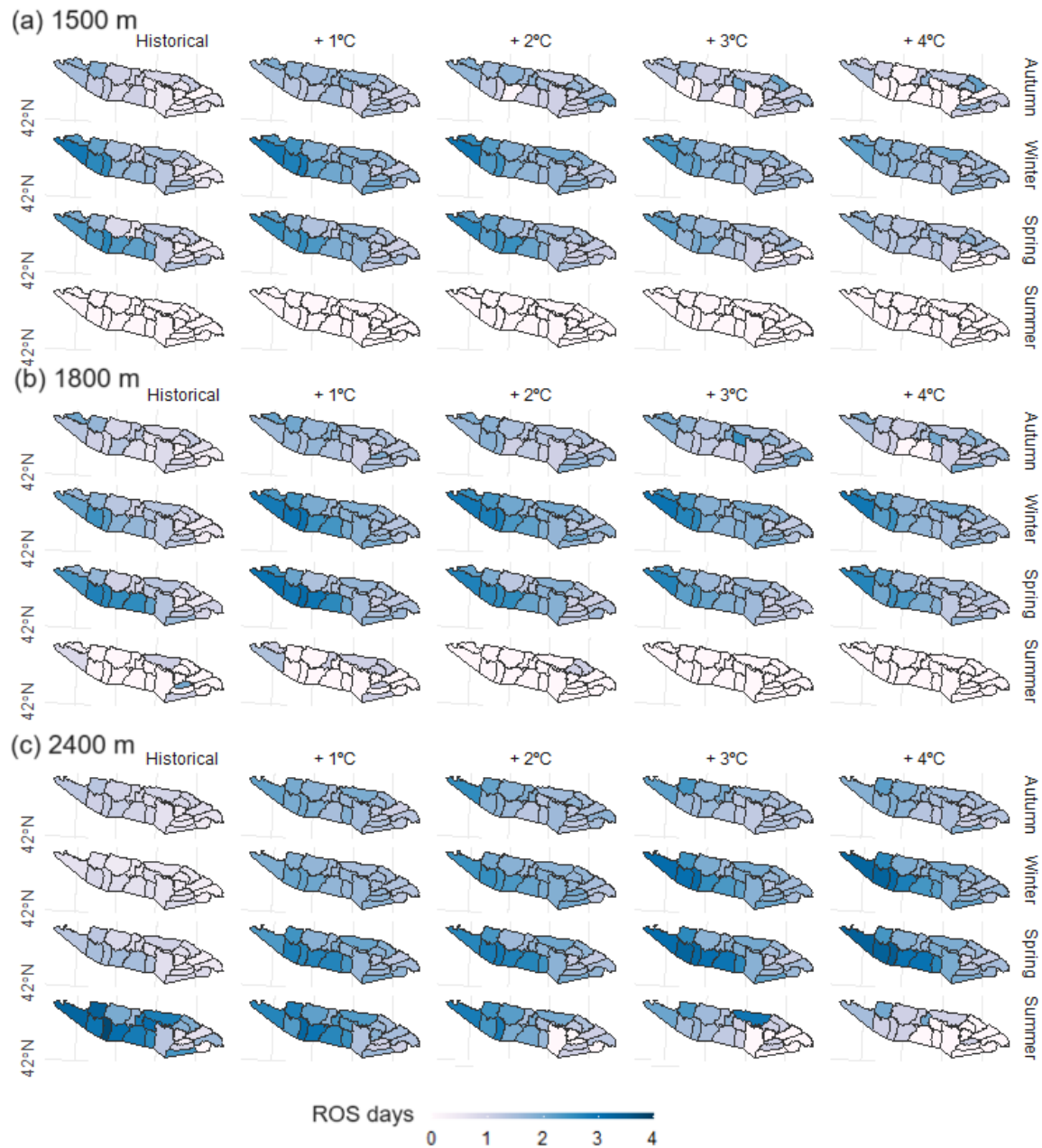


**Figure 5.** Average ROS frequency (days) for a season for (a) 1500 m, (b) 1800 m and (c) 2400 m elevation. Data are shown for the historical climate period (1980 – 2019) and increment of temperature (left to right). Data are the average of the simulated precipitation change (from -10% to 10%, by steps of 10%).

### 4.3 ROS rainfall amount

The spatial and temporal distribution of ROS rainfall amount is presented in Figure 6 and 7. The average 1500 m elevation ROS rainfall amount by year is 23, 28, 21, and 20 mm/day for SW, SE, NW, NE sectors, respectively. At 1800 m elevation, the highest ROS rainfall amount values are also found in SE (29 mm/day). Particularly, SE sector experiences the highest ROS rainfall amount during autumn and summer (around 40 mm/day at 1500 m and 1800 m elevations). At 2400 m elevation, however, maximum ROS rainfall amount values are found in SW and NW during autumn. Here, the largest ROS rainfall amount spatial and seasonal

299 distribution ranges from SW (29 mm/day, autumn), NW (28 mm/day, summer), SE (24 mm/day, autumn) to  
 300 NE (23 mm/day, autumn).

301  
 302  
 303



304  
 305  
 306  
 307  
 308  
 309

**Figure 6.** Average ROS rainfall amount (mm/day) for each month of the season. Data are shown for the historical climate period (1980 – 2019) and different increments of temperature (colors), grouped by month (x-axis), elevation and sector (boxes). Data are the average of the simulated precipitation change (from -10% to 10%, by steps of 10%).

310 ROS rainfall amount progressively increases due to warming (4%, 4%, and 5% per °C for 1500 m, 1800 m,  
 311 and 2400 m elevations, respectively; Table S2). Small differences are found by elevation and sector. 1500 m  
 312 elevation ROS rainfall amount increases until + 3°C, and generally decreases for + 4°C during the earliest  
 313 (October to December) and latest (April and May) months of the snow season. Similar patterns are found at  
 314 1800 m elevation. ROS rainfall amount increases up to + 4°C, except in the SE sector for specific months  
 315 (Figure 6). The latest sector shows also maximum ROS rainfall amount values in autumn due to torrential  
 316 rainfall. 2400 m elevation ROS rainfall amount increase at a constant rate of around 5 % per °C. Yet, maximum  
 317 increases are simulated in SW during summer, when ROS rainfall amount almost doubles the historical climate  
 318 period (+ 40% for + 4°C).

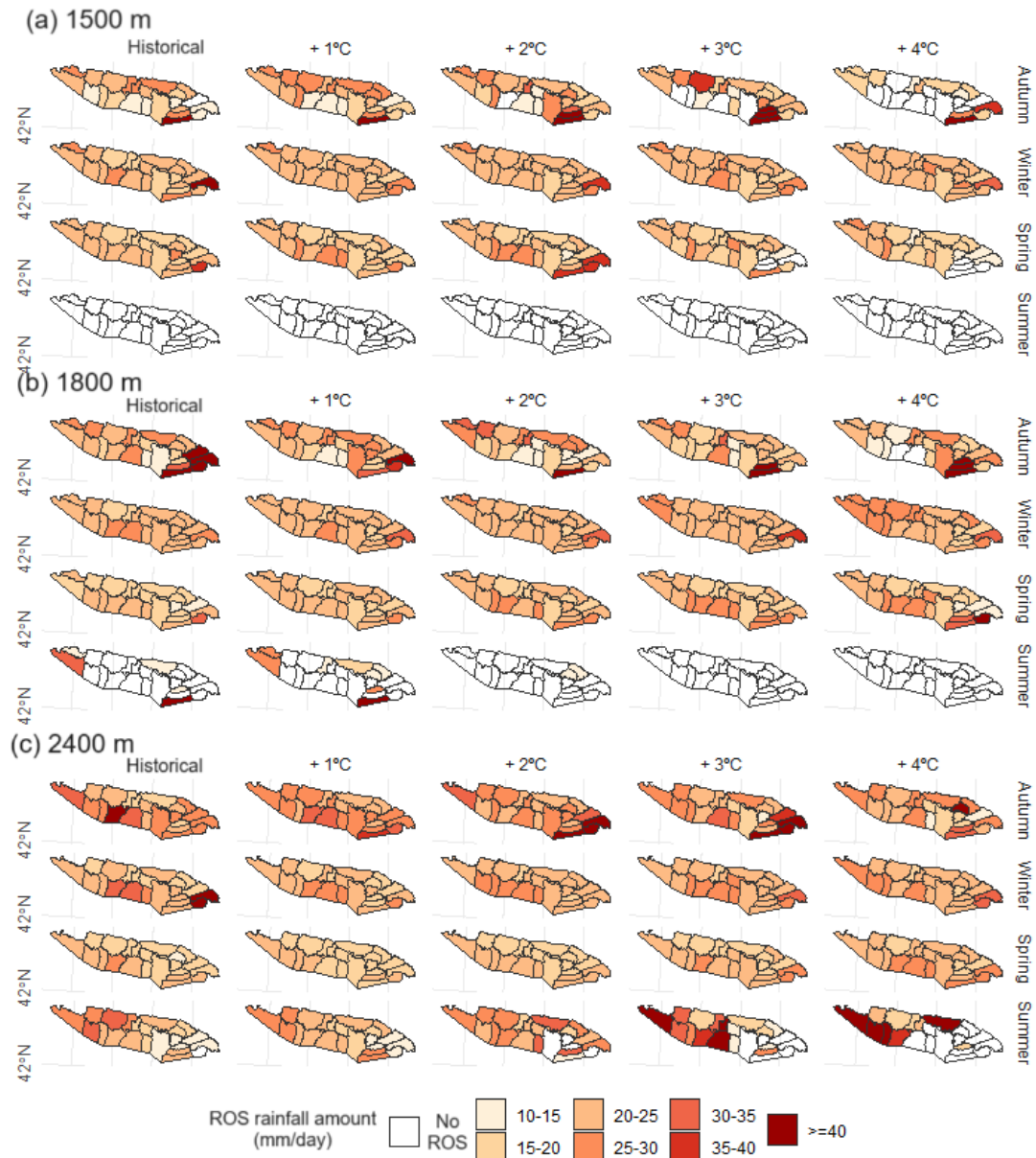
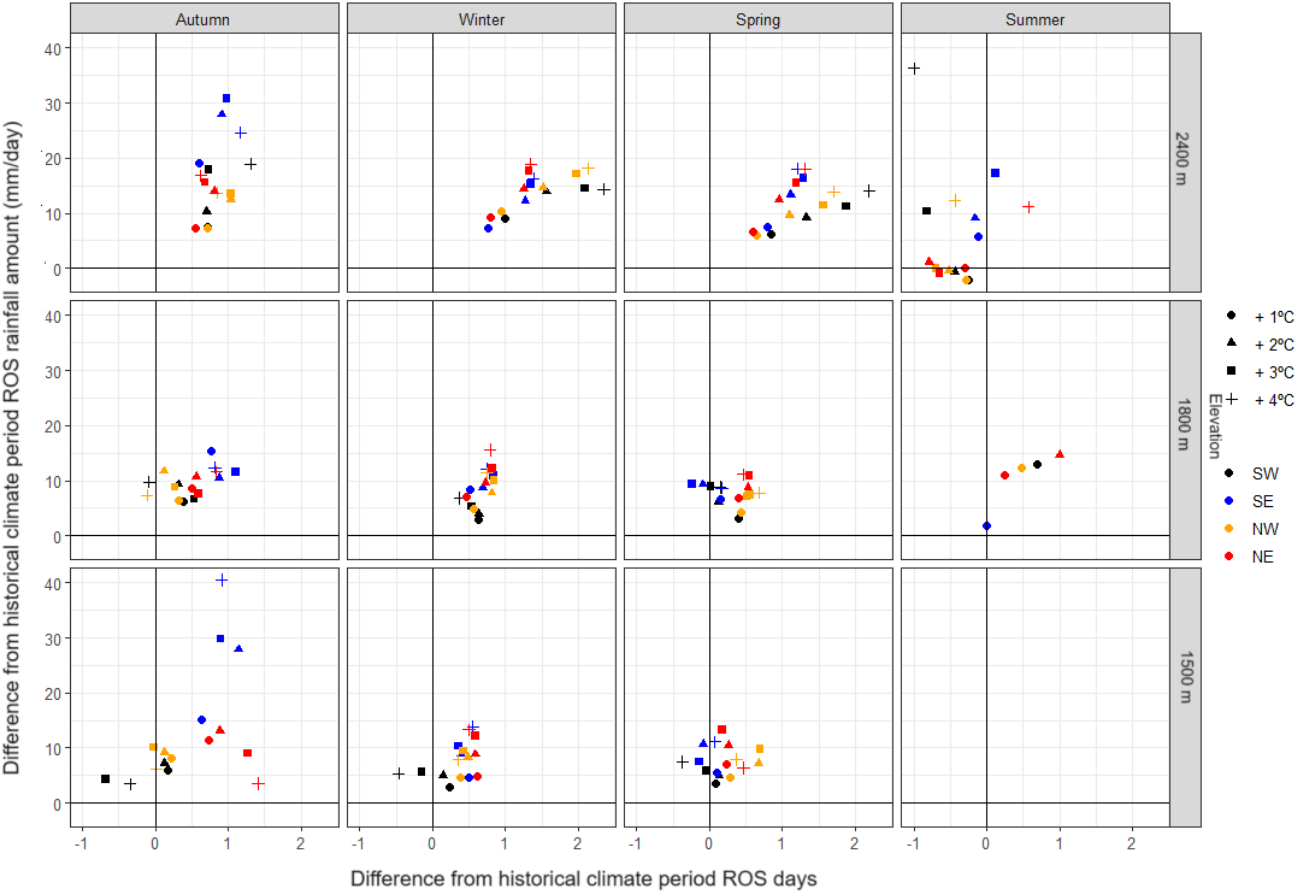


**Figure 7.** Average ROS rainfall amount (mm/day) for a season (rows) for (a) 1500 m, (b) 1800 m and (c) 2400 m elevation. Data are shown for the historical climate period (1980 – 2019) and increment of temperature (columns). Data are the average of the simulated precipitation change (from -10% to 10%, by steps of 10%).

333 The minimum differences between sectors are detected in these seasons. In summer, ROS rainfall amount and  
 334 frequency tends to generally decrease for all elevations under severe warming due to snow cover depletion.  
 335  
 336  
 337



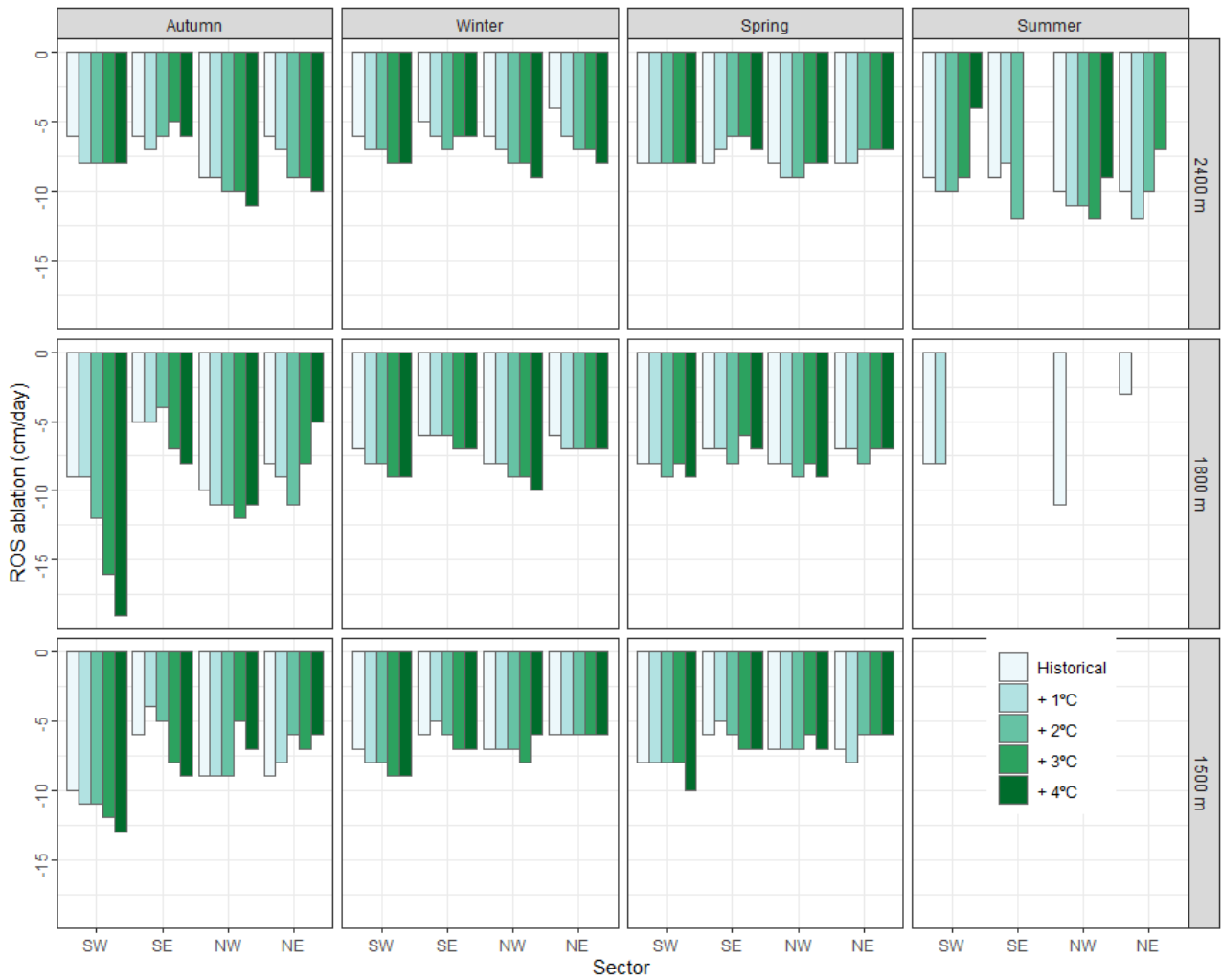
338  
 339 **Figure 8.** Scatterplot between ROS rainfall amount (mm/day) difference from the historical climate period  
 340 (1980 – 2019) (y-axis) and ROS days difference from the historical climate period (x-axis). Data is  
 341 calculated by the average difference between (a) the historical climate period values and (b) the values  
 342 resulting from the different increments of temperature, only for the massifs where ROS frequency exists on  
 343 (a) and (b). Data are shown for each season (columns), elevation (rows), sector (color) and increment of  
 344 temperature (point shape). Data are the average of the simulated precipitation change (from -10% to 10%, by  
 345 steps of 10%).

#### 346 347 4.4. ROS ablation

348  
 349 ROS ablation is presented at Figure 9 and 10. ROS ablation ranges from -10 cm/day in NW 2400 m elevation  
 350 (summer) to – 5 cm/day in NE 2400 m elevation (winter). ROS ablation nearly doubles the average daily snow  
 351 ablation for all days on a season (Figure S5). Comparison with the reference baseline period reveals contrasting  
 352 ROS ablation changes depending on the season, elevation and sector. Overall ROS ablation progressively

353 increases due to warming in coldest zones and months of the season. The largest ROS ablation increments are  
 354 detected in autumn and winter. For the former, ROS ablation increases at a generally constant rate in SW (11 %)   
 355 NE (19 %) and NW (4 % per °C). For the latter, ROS ablation increases also in SW (11 %), NW (14 %) and   
 356 NE (34 % per °C). In detail, maximum ROS ablation due to warming is found for 1800 m elevation during   
 357 autumn (Figure 9). ROS ablation exhibit slow and no-changes in the warmest zone (SE), as well in the warmest   
 358 months of the season, regardless the elevation band.

359  
 360  
 361  
 362



363  
 364 **Figure 9.** ROS ablation (cm/day; y-axis) for the historical climate period (1980 – 2019) and increment of  
 365 temperature (colors), sector (x-axis), season (columns) and elevation (rows). Data are the average of the  
 366 simulated precipitation change (from -10% to 10%, by steps of 10%).



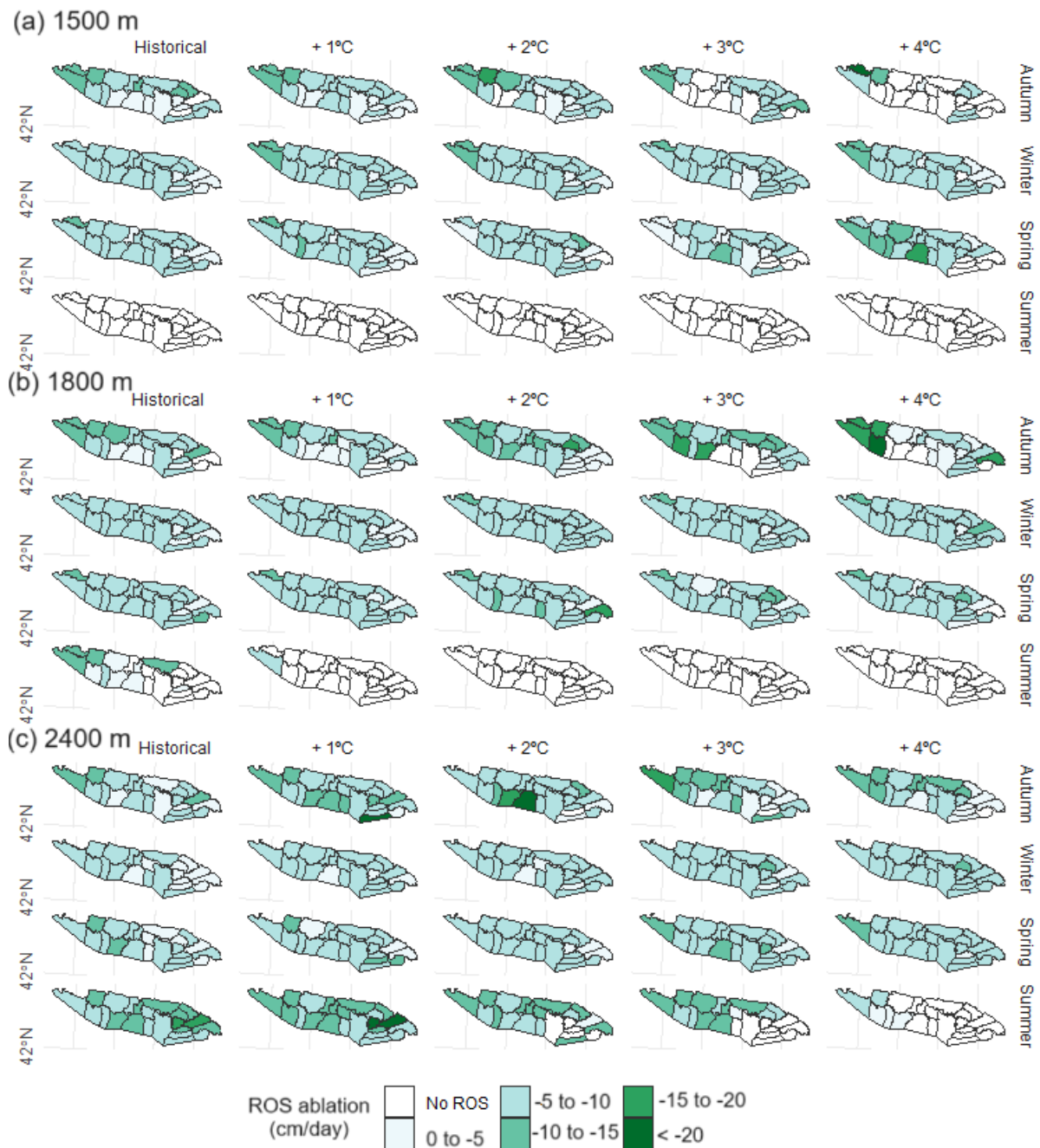


**Figure 10.** Average ROS ablation (cm/day) for (a) 1500 m, (b) 1800 m and (c) 2400 m elevation. Data are shown for the historical climate period (1980 – 2019) and increment of temperature (columns). Data are the average of the simulated precipitation change (from -10% to 10%, by steps of 10%).

## 5 Discussion

378 The Pyrenees experienced a statistically significant positive temperature trend since the 1980s (ca. + 0.2  
 379 °C/decade) but no statistically significant precipitation trends are detected (OPCC, 2018) due to strong spatial  
 380 (Vicente-Serrano et al., 2017), inter-annual and long-term variability of the latter (Peña-Angulo et al., 2021).  
 381 Depending on the study period different snow trends were found. From ca. 1980 to 2010, non-statistically  
 382 significant snow days and snow accumulation positive trends were generally detected at > 1000 m (Buisan et  
 383 al., 2016), 1800 m (Serrano-Notivoli et al., 2018), and > 2000 m (Bonsoms et al., 2021a). Long-term trends  
 384 (1957 to 2017), however, reveal statistically significant snow depth decreases at 2100 m, but large variability  
 385 depending on the sector and the snow indicator (López-Moreno et al., 2020). Climate projections for the end  
 386 of the 21<sup>st</sup> century suggest an increase of temperature (> 3°C), together with 1500 m precipitation shifts (<  
 387 10%) from autumn to spring (Amblar-Francés et al., 2020). Within this climate context, ROS spatio-temporal  
 388 patterns will likely change. In order to anticipate future ROS patterns, we analyzed ROS sensitivity to warming  
 389 through three key indicators of frequency, rainfall intensity and snow ablation.

390

### 391 **5.1 ROS spatial variability**

392

393 The climatic setting of the Pyrenees as well as its relief configuration determines a remarkable spatial and  
 394 temporal variability of ROS events. HS decrease by 39 %, 37 % and 28 % per °C, for 1500 m, 1800 m and  
 395 2400 m elevations, respectively. Similarly, Sf decreases by 29 %, 22 %, and 12 % per °C for 1500 m, 1800 m,  
 396 and 2400 m elevations. These results provide evidence of an elevation-dependent snow sensitivity to  
 397 temperature change and are consistent with snow sensitivity to climate works in near alpine sectors, such as  
 398 the Alps (e.g., Martin et al., 1994). HS and Sf maximum reductions are reached for 1°C of warming, suggesting  
 399 non-linear HS decreases, in accordance with previous snow sensitivity to climate change reported in central  
 400 Pyrenees (López-Moreno et al., 2013). The generally ROS rainfall amount increase reported in this work,  
 401 independently of the increment of temperature and elevation, is explained by the Sf reduction expected for all  
 402 sectors (Figure 3). Large increments of warming decreases ROS frequency due to snow cover depletion in  
 403 early autumn and late spring (Figure 2). However, for the rest of the seasons and even with snow cover  
 404 reductions, the snowpack does not fully disappear leading to ROS frequency increases due to more rainy days.

405

406 SW and NW annual ROS frequency almost doubles (17 and 12 days/year, respectively) the one recorded in SE  
 407 and NE (9 days/year, for both sectors). Maximum ROS frequency for a season is found in SW and NW because  
 408 of larger snowpacks in this sector (i.e., López-Moreno, 2005; López-Moreno et al, 2007; Navarro-Serrano et  
 409 al., 2017; Bonsoms et al., 2021a). Thus, snow cover last longer until spring when minimum Sf values are found  
 410 (Figure 2). SW and NW sectors are the most exposed to SW and W air flows (negative NAO phases) (López-  
 411 Moreno, 2005), which bring wet and mild conditions over the mountain range, leading to most ROS-related  
 412 floods in the range (Morán-Tejeda et al., 2019). Maximum ROS rainfall amount is generally detected in May,  
 413 except in NE (at 2400 m elevation) and SE (all elevations). In the latter sectors, ROS rainfall amount tends to  
 414 disappear in October under large (> 2°C) increments of temperature. The seasonal snow accumulation in NE  
 415 and SE is lower-than-average due to the lower influence of Atlantic climate in these sectors of the range. In

addition, the SE is closer to the 0°C due to higher-than-average sublimation, latent and radiative heat fluxes (Bonsoms et al., 2022) and for this reason in this sector each increment of temperature has larger effects on the Sf, HS and ROS frequency reduction (Figure 3). 2400 m elevation shows the largest variation over the historical climate period as well as ROS rainfall amount and frequency (Figure 8) because of the larger snowpack and duration compared to 1500 m and 1800 m areas. Thus, 2400 m elevation snow duration last until spring and summer, when the largest shift from snowfall to rainfall is found. On the other hand, 1800 m elevation shows the maximum ROS rainfall amount since the amount of moisture for condensation decreases while air masses increase height (Roe and Baker, 2006). The largest ROS rainfall amount is detected in SE during autumn (Figure 7). This sector is exposed to Mediterranean low-pressure systems (negative WeMO phases), that usually trigger heavy rainfall events (Lemus-Canovas et al., 2021) during this season, when snow cover may have already developed at sufficiently high elevation.

427

## 5.2 ROS comparison with other studies

429

Recent ROS trends in other mid-latitude areas are in accordance with ROS analysis presented here. Freudiger et al. (2013) analyzed the ROS trends (1950 – 2011 period) of the Rhine, Danube, Elbe, Weser, Oder, and Ems (Central Europe) basins. They found an overall ROS frequency increase during January and February (1990 to 2011 period), which is consistent with the ROS rainfall amount and frequency increase simulated in winter for the Pyrenees for all elevations and increment of temperature. Similarly, in Sitter River (NE Switzerland), a ROS frequency increase of around 40% (200%) at <1500 m (>2500 m) was detected between 1960 and 2015 (Beniston and Stoffel, 2016). During the last half of the 20<sup>th</sup> century, ROS frequency trends show an upward (downward) trend in high (low) elevation in western United-States (McCabe et al., 2007), as well as in southern British Columbia (Loukas et al., 2002) and at catchment scale in Oregon (United-States) (Surfleet and Tullos, 2013). Same ROS frequency increases (decreases) has been detected from 1980 to 2010 in Norwegian at high (low) elevated mountain zones (Pall et al., 2019). However, in contradiction with our results and previous studies, winter Northern-Hemisphere ROS frequency trends (1979-2014 period) show no-clear trends (Cohen et al., 2015).

443

Results exposed in this work provide more evidence of ROS frequency increases in high-elevation zones, as it has been suggested by climate projections and ROS sensitivity to temperature studies. ROS shows an elevation-dependent pattern that was previously reported in the Swiss Alps (Morán-Tejeda et al., 2016). In Sitter River (NE Switzerland), an increase of 2 to 4 °C over the 1960 to 2015 period results in an increase of the ROS frequency by around 50% at > 2500 m (Beniston and Stoffel, 2016). Likewise, 21st century high-emission scenarios (RCP8.5), suggest increases in ROS frequency and intensity in Gletsch (Switzerland) high-elevation area. Other studies suggest that on climate projections for ROS definitions that include snow melting (Musselman et al., 2018), natural climate variability contributes to a large extend (70 %) of ROS variability (Schirmer et al., 2022). Li et al. (2019) analyzed the future ROS frequency in the conterminous United-States and detected a nonlinear trend ROS due to warming, which is consistent with the different ROS rainfall amount

and frequency responses depending on the increment of temperature detected in our work. Climate projections for the mid-end of the 21<sup>st</sup> century projected positive ROS frequency and rainfall trends in Western United-States and Canada (Jeong and Sushama, 2018). Similarly, ROS frequency will likely decrease (increase) in the warmest months of the season in low (high) elevation areas of western United-States (Musselman et al., 2018). The same is projected Norwegian mountains (Mooney and Li, 2021). López-Moreno et al. (2021) analyzed 40 worldwide basins ROS sensitivity to warming. In their study they found a decrease of ROS events in warm mountain areas. However, they detected ROS frequency increases in cold-climate mountains where large snow accumulation is found despite warming. In accordance with our results, they identified large seasonal differences and ROS frequency decreases in Mediterranean mountains due to snow cover depletion in the last months of the snow season.

### 5.3 ROS ablation

Warming increases ROS ablation from autumn to winter on deep snowpacks and in the coldest sectors of the range, due to higher energy for snow ablation and closer 0°C isotherm conditions in a warmer than the historical climate period. Data show no-changes and decreases in ROS ablation in SE and spring since the snowpack is already near to the isothermal conditions. These results go in line with results observed for cold and warm Pyrenean sites (López-Moreno et al., 2013) as well as for different Northern-Hemisphere sites (Essery et al., 2020). ROS ablation indicator is also indirectly affected by the HS magnitude decreases (30 % per °C; Figure 3), and therefore lower ROS ablation is directly affected by lower HS magnitudes. Previous literature pointed out that warming have different effects on snow ablation patterns. Higher than average temperatures advance the peak HS date on average 5 days per °C in 1800 m and 2400 m elevations (Bonsoms et al., 2023), triggering earlier snow ablation onsets, and therefore lower solar radiation fluxes (López-Moreno et al., 2013; Lundquist et al., 2013; Pomeroy et al., 2015; Musselman et al., 2017a; Sanmiguel-Valellado et al., 2022), as well as earlier snow depletion before the maximum advection of heat fluxes into the snowpack (spring) (Bonsoms et al., 2022). Slower snow melt rates in a warmer climate have been detected in Western United-States (Musselman et al., 2017), as well as the entire Northern-Hemisphere (Wu et al., 2018). Low or inexistent changes in snow ablation on warm and marginal snowpacks has been previously detected in the central Pyrenees (López-Moreno et al., 2013), in forest and open areas (Sanmiguel-Valellado et al., 2022), in the entire range (Bonsoms et al., 2022), and other Iberian Peninsula Mountain ranges outside the Pyrenees (Alonso-González et al., 2020a).

ROS ablation is larger than the average snow ablation during a snow ablation day (Figure S5) due to higher SEB positive fluxes. Several works analyzed SEB changes on ROS events, and different SEB contributions has been found depending on the geographical area (Mazurkiewicz et al., 2008; Garvelmann et al., 2014b; Würzer et al., 2016; Corripio and López-Moreno, 2017; Li et al., 2019), ranging from net radiation in Pacific North West (Mazurkiewicz et al., 2008) to LWin and turbulent heat fluxes in conterminous United-States

mountain areas (Li et al., 2019) or the Swiss Alps (e.g., Würzer et al., 2016). In general, studies in mid-latitude mountain ranges have shown that turbulent heat fluxes contribute between 60 and 90 % of the energy available for snow ablation during ROS days (e.g., Marks et al., 1998; Garvelmann et al. 2014; Corripio and López-Moreno, 2017). In the central Pyrenees (at > 2000 m) the meteorological analysis of a ROS event reveals that ROS ablation is larger than a normal ablation day because of the large advection of LWin and especially sensible heat fluxes (Corripio and López-Moreno, 2017). LWin increases due to the high cloud cover and warm air, as it is frequently observed during ROS episodes (Moore and Owens, 1984). Further works should analyze the SEB controls during ROS events within the entire mountain range, as well as the ROS hydrological responses to climate warming.

#### **5.4 ROS socio-environmental impacts and hazards**

Temperature-induced changes in the seasonal snowpack and during ROS days suggest several hydrological shifts including, but not limited to, earlier peak flows on the season (Surfleet and Tullos, 2013), rapid streamflow peaks during high precipitation events in frozen soils (Shanley and Chalmers, 1999), faster soil moisture depletion and lower river discharges in spring due to earlier snow melt in the season (Stewart, 2009). The shortening of the snow season due to warming reported in this work will potentially alter alpine phenological patterns (i.e., Wipf and Rixen, 2010) and expand forest cover (Szczypta et al., 2015). Although vegetation branches intercept a large amount of snowfall, intermediate and high vegetation shields short-wave radiation, reduces snow wind-transport and turbulent heat fluxes (López-Moreno and Latron, 2008; Sanmiguel-Valellado et al., 2022). Snow-forest interactions, their sensitivity to climate change as well as the ROS hydrological response within a changing landscape is far from understood across the range and should be the base of forthcoming works.

The higher ROS rainfall amount and frequency (Figure 8) will likely imply an increase of ROS-related hazards and impacts in the mountain ecosystem. Heavy ROS rainfall amount changes snow metamorphism on saturated snowpacks and leads to high-speed water percolation (Singh et al., 1997). The subsequent water refreezing changes the snowpack conditions and creates an ice-layer in the snowpack that can reach the surface (Rennert et al., 2009). ROS can cause plant damage (Bjerke et al., 2017) and the ice encapsulation of vegetation in tundra ecosystems can trigger severe wildlife impacts, such as vertebrate herbivores starvation, reindeer population mortality (Kohler and Aanes, 2004) and higher competition between species (Hansen et al 2014). Nevertheless, any study to the date analyzed ROS-related impacts in flora and fauna across Southern-European mountains. Snow albedo decay due positive heat fluxes and rainfall in ROS events (Corripio and López-Moreno, 2017), lead to faster snow ablation even on the next days (e.g., Singh et al. 1997). The combination of changes in internal snowpack processes, larger ROS rainfall amount, and more energy to ablate snow during spring could enhance snow runoff, especially during warm and wet snowpack conditions (Würzer et al., 2016). In snow-dominated regions ROS can lead to a specific type of avalanching (Conway and Raymond, 1993) and floods (Surfleet and Tullos, 2013). The latter are the most environmental damaging risk in Spain (Llasat et al.,

2014) and around 50% of the flood in the Iberian Peninsula are due to ROS events (Morán-Tejeda et al., 2019). More than half of the historical (1940 to 2012) flood events in the Ésera river catchment (central Pyrenees) occurred during spring (Serrano-Notivol et al., 2017), which coincides with the snow ablation season. ROS floods have also economic impacts. For instance, a ROS flood event that occurred on 13<sup>th</sup> June of 2013 in the Garonne River (Val d'Aran, central Pyrenees) cost approximately 20 million of euros to the public insurance (Llasat et al., 2014).

## 5.5 Limitations

This study evaluates the sensitivity of ROS responses to climate change, enabling a better understanding of the non-linear ROS spatiotemporal variations in different sectors and elevations of the Pyrenees. Instead of presenting diverse outputs from climate model ensembles (López-Moreno et al., 2010), we provide ROS sensitivity values per 1°C, making them comparable to other regions and seasons. The temperature and precipitation change values used in this sensitivity analysis are based on established climate projections for the region (Amblar-Francés et al., 2020). Precipitation projections in the Pyrenees, however, exhibit high uncertainties among different models, emission scenarios, and temporal periods (López-Moreno et al., 2008).

The SAFRAN meteorological system used in this work relies on a topographical spatial division and exhibit and accuracy of around 1 °C in air temperature and around 20 mm in the monthly cumulative precipitation (Vernay et al., 2022). Precipitation phase partitioning methods are subject to uncertainties under close-to-isothermal conditions (Harder and Pomeroy, 2014). Hydrological models are also subject to errors in the snowpack prediction (Essery, 2015). However, the FSM2 is a multiphysics snowpack model that has been validated previously in the Pyrenees (Bonsoms et al., 2023) and compared against different snowpack models (Krinner et al., 2018), providing evidence of its robustness.

## 6 Conclusions

The expected decreases in snowfall fraction (Sf) and height of snow (HS) due to climate warming will likely change ROS spatio-temporal patterns across the Pyrenees. Therefore, a better understanding of ROS is required. This work analyzed the ROS sensitivity to warming by forcing a physically based snow model with perturbed reanalysis climate data (1980 – 2019 period) for 1500 m, 1800 m and 2400 m elevation areas of the Pyrenees. ROS sensitivity to temperature and precipitation is evaluated by frequency, rainfall intensity and snow ablation during ROS days.

During the historical climate period, annual ROS frequency totals on average 10, 12 and 10 day/season for 1500 m, 1800 m and 2400 m elevations. Higher-than-average annual ROS frequency are found in 1800 m elevation SW (17 days/year) and NW (12 days/year), which contrast with the minimums detected in SE (9 days/year). The different spatial and seasonal ROS response to warming suggest that contrasting and shifting

trends could be expected in the future. Overall ROS frequency decreases during summer at 2400 m elevation for  $> 1^{\circ}\text{C}$ . When temperature is progressively increased the greatest ROS frequency increases are found for SW 2400 m elevation (around 1 day/month for  $+ 1^{\circ}\text{C}$ ). ROS frequency is highly sensitive to warming in the snow onset and offset months when diverging factors play a key role. On the one hand, maximum Sf decreases are simulated for spring, leading to rainfall increases; on the other hand, warming depletes the snowpack in the warmest and snow driest sectors of the range. Consequently, data suggest a general ROS frequency decrease for most of the SE massifs, where the snowpack is near the isothermal conditions in the historical climate period. Yet, during spring, the highest ROS frequency increases are detected in SW and NW, since these sectors are less exposed to radiative and turbulent heat fluxes and record higher-than-average seasonal snow accumulations.

ROS rainfall amount generally increases due to warming, independently of the sector and elevation, being limited by the number of ROS days. The largest and constant increments are observed in spring, when ROS rainfall amount increases at a rate of 7, 6 and 3 % per  $^{\circ}\text{C}$  for 1500 m, 1800 m and 2400 m, respectively. ROS rainfall amount increases is influenced by Sf reductions, which decrease at a rate of 29 %, 22 %, and 12 % per  $^{\circ}\text{C}$  for 1500 m, 1800 m, and 2400 m elevations, respectively. ROS rainfall amount maximum values are detected in SE (28 mm/day), especially in 1800 m elevation during autumn (45 mm/day), since this sector is exposed to subtropical Mediterranean flows.

Finally, ROS ablation shows contrasting patterns depending on the season, sector and elevation. Generally, ROS ablation increases in cold snowpacks, such as those simulated in 2400 m elevation and during cold seasons (autumn and winter). Here, ROS ablation follows a constant ablation rate of around  $+ 10\%$  per  $^{\circ}\text{C}$ , due to higher-than-average positive sensible and LWIn heat fluxes. However, in SE and 1500 m elevation, where marginal and isothermal snowpacks are found, no changes or decreases in ROS ablation are detected due to snowpack reductions in a warmer climate. Results demonstrate the high snow sensitivity to climate within a mid-latitude mountain range and suggest significant changes with regards to water resources management. Relevant implications in the ecosystem and socio-economic activities associated with snow cover are anticipated.

## **Data availability**

FSM2 is an open access snow model (Essery, 2015) provided at <https://github.com/RichardEssery/FSM2> (last access 15 January 2023). SAFRAN climate dataset (Vernay et al., 2022) is available by AERIS at <https://www.aeris-data.fr/landing-page/?uuid=865730e8-edeb-4c6b-ae58-80f95166509b#v2020.2> (last access 16 December 2022). Data of this work is available upon request by the first author ([josepbonsoms5@ub.edu](mailto:josepbonsoms5@ub.edu)).

## **Author contribution**

J.B., J.I.L.M., and E.A.G. designed the work. J.B. analyzed the data and wrote the manuscript. J.B., J.I.L.M.,

595 E.A.G., C.D.B., and M.O. provided feedback and edited the manuscript. J.I.L.M., M.O. supervised the project  
596 and acquired funding.

## 597 **Competing interests**

598 The authors declare that they have no conflict of interest.

## 599 **Acknowledgements**

600 This work frames within the research topics examined by the research group “Antarctic, Artic, Alpine  
601 Environments-ANTALP” (2017-SGR-1102) funded by the Government of Catalonia, HIDROIBERNIEVE  
602 (CGL2017-82216-R) and MARGISNOW (PID2021-124220OB-100), from the Spanish Ministry of Science,  
603 Innovation and Universities. JB is supported by a pre-doctoral University Professor FPI grant (PRE2021-  
604 097046) funded by the Spanish Ministry of Science, Innovation and Universities. The authors are grateful to  
605 Pascal Haegeli, Samuel Morin and an anonymous reviewer for their review of this manuscript.

## 606 607 **References**

- 608  
609 Alonso-González, E., Aalstad, K., Baba, M. W., Revuelto, J., López-Moreno, J. I., Fiddes, J., et al. MuSA: The  
610 Multiscale Snow Data Assimilation System (v1.0). *Geoscientific Model Development Discussions*, 1–43.  
611 <https://doi.org/10.5194/gmd-2022-137> , 2022.  
612  
613 Alonso-González, E., López-Moreno, J.I., Navarro-Serrano, F., Sanmiguel-Valladolid, A., Aznárez-Balta, M.,  
614 Revuelto, J., and Ceballos, A.: Snowpack Sensitivity to Temperature, Precipitation, and Solar Radiation  
615 Variability over an Elevational Gradient in the Iberian Mountains, *Atmos. Res.*, 243, 104973 [https://doi.org/](https://doi.org/10.1016/j.atmosres.2020.104973)  
616 10.1016/j.atmosres.2020.104973, 2020a.  
617  
618 Alonso-González, E., López-Moreno, J.I., Navarro-Serrano, F., Sanmiguel-Valladolid, A., Revuelto, J.,  
619 Domínguez-Castro, F., and Ceballos, A.: Snow climatology for the mountains in the Iberian Peninsula using  
620 satellite imagery and simulations with dynamically downscaled reanalysis data, *International Journal of*  
621 *Climatology*, 40(1), 477–491, <https://doi.org/10.1002/joc.6223>, 2019.  
622  
623 Alonso-González, E., López-Moreno, J. I., Navarro-Serrano, F. M., and Revuelto, J.: Impact of North Atlantic  
624 Oscillation on the snowpack in Iberian Peninsula mountains, *Water (Switzerland)*, 12,  
625 <https://doi.org/10.3390/w12010105>, 2020b.  
626  
627 Amblar-Francés, M. P., Ramos-Calzado, P., Sanchis-Lladó, J., Hernanz-Lázaro, A., Peral-García, M. C.,  
628 Navascués, B., Dominguez-Alonso, M., Pastor-Saavedra, M. A., and Rodríguez-Camino, E.: High resolution  
629 climate change projections for the Pyrenees region, in: *Advances in Science and Research*, 191–208,  
630 <https://doi.org/10.5194/asr-17-191-2020>, 2020.  
631  
632 Barnett, T.P., Adam, J.C., and Lettenmaier, D.P., Potential impacts of a warming climate on water availability  
633 in snow-dominated regions. *Nature*. <https://doi.org/10.1038/nature04141>, 2005.  
634  
635 Bartsch, A., Kumpula, T., Forbes, B. C., and Stammer, F.: Detection of snow surface thawing and refreezing  
636 in the Eurasian arctic with QuikSCAT: Implications for reindeer herding, *Ecological Applications*, 20, 2346–  
637 2358, <https://doi.org/10.1890/09-1927.1>, 2010.



- 636 Beniston, M. and Stoffel, M.: Rain-on-snow events, floods and climate change in the Alps: Events may increase  
637 with warming up to 4 °C and decrease thereafter, *Science of the Total Environment*, 571, 228–236,  
638 <https://doi.org/10.1016/j.scitotenv.2016.07.146>, 2016.
- 639 Beniston, M., Farinotti, D., Stoffel, M., Andreassen, L. M., Coppola, E., Eckert, N., Fantini, A., Giacona, F.,  
640 Hauck, C., Huss, M., Huwald, H., Lehning, M., López-Moreno, J. I., Magnusson, J., Marty, C., Morán-Tejeda,  
641 E., Morin, S., Naaim, M., Provenzale, A., Rabatel, A., Six, D., Stötter, J., Strasser, U., Terzago, S., and Vincent,  
642 C.: The European mountain cryosphere: A review of its current state, trends, and future challenges,  
643 <https://doi.org/10.5194/tc-12-759-2018>, 2018.
- 644 Bieniek, P. A., Bhatt, U. S., Walsh, J. E., Lader, R., Griffith, B., Roach, J. K., and Thoman, R. L.: Assessment  
645 of Alaska rain-on-snow events using dynamical downscaling, *J Appl Meteorol Climatol*, 57, 1847–1863,  
646 <https://doi.org/10.1175/JAMC-D-17-0276.1>, 2018.
- 647 Bintanja, R. and Andry, O.: Towards a rain-dominated Arctic, *Nat Clim Chang*, 7, 263–267,  
648 <https://doi.org/10.1038/nclimate3240>, 2017.
- 649 Bonsoms, J., Franch, F. S., and Oliva, M.: Snowfall and snow cover evolution in the eastern pre-pyrenees (Ne  
650 iberian peninsula), *Geographical Research Letters*, 47, 291–307, <https://doi.org/10.18172/cig.4879>, 2021a.
- 651 Bonsoms, J., González, S., Prohom, M., Esteban, P., Salvador-Franch, F., López-Moreno, J. I., and Oliva, M.:  
652 Spatio-temporal patterns of snow in the Catalan Pyrenees (NE Iberia), *International Journal of Climatology*,  
653 41, 5676–5697, <https://doi.org/10.1002/joc.7147>, 2021b.
- 654 Bonsoms, J., López-Moreno, J. I., González, S., and Oliva, M.: Increase of the energy available for snow  
655 ablation in the Pyrenees (1959–2020) and its relation to atmospheric circulation, *Atmos Res*, 275,  
656 <https://doi.org/10.1016/j.atmosres.2022.106228>, 2022a.
- 657 Bonsoms, J., López-Moreno, J. I., and Alonso-González, E.: Snow sensitivity to temperature and precipitation  
658 change during compound cold-hot and wet-dry seasons in the Pyrenees, *The Cryosphere*, 17, 1307–1326,  
659 <https://doi.org/10.5194/tc-17-1307-2023>, 2023.
- 660 Buisan, S.T., López-Moreno, J.I., Sanz, M.A. and Korchendorfer, J. Impact of weather type variability on  
661 winter precipitation, temperature and annual snowpack in the Spanish Pyrenees. *Climate Research*, 69, 79–92.  
662 <https://doi.org/10.3354/cr01391>, 2016.
- 663 Bjerke JW, Treharne R, Vikhamar-Schuler D, Karlsen S R, Ravolainen V, Bokhorst S, Phoenix G K, Bochenek  
664 Z and Tømmervik H 2017 Understanding the drivers of extensive plant damage in boreal and Arctic  
665 ecosystems: insights from field surveys in the aftermath of damage *Sci. Total Environ.* 599 1965–76.
- 666 Ceron, J. P., Tanguy, G., Franchistéguy, L., Martin, E., Regimbeau, F., and Vidal, J. P.: Hydrological seasonal  
667 forecast over France: Feasibility and prospects, *Atmospheric Science Letters*, 11, 78–82,  
668 <https://doi.org/10.1002/asl.256>, 2010.
- 669 Cohen, J., Ye, H., and Jones, J.: Trends and variability in rain-on-snow events, *Geophys Res Lett*, 42, 7115–  
670 7122, <https://doi.org/10.1002/2015GL065320>, 2015.
- 671 Collados-Lara, A. J., Pulido-Velazquez, D., Pardo-Igúzquiza, E., and Alonso-González, E.: Estimation of the  
672 spatio-temporal dynamic of snow water equivalent at mountain range scale under data scarcity, *Science of the*  
673 *Total Environment*, 741, <https://doi.org/10.1016/j.scitotenv.2020.140485>, 2020.
- 674 Conway, H. and Raymond, C. F.: Snow stability during rain, *Journal of Glaciology*, 39, 635–642,

675 <https://doi.org/10.3189/s0022143000016531>, 1993.

676 Corripio, J. G. and López-Moreno, J. I.: Analysis and predictability of the hydrological response of mountain  
677 catchments to heavy rain on snow events: A case study in the Spanish Pyrenees, *Hydrology*, 4,  
678 <https://doi.org/10.3390/hydrology4020020>, 2017.

679 Crawford, A. D., Alley, K. E., Cooke, A. M., and Serreze, M. C.: Synoptic Climatology of Rain-on-Snow  
680 Events in Alaska, <https://doi.org/10.1175/MWR-D-19>, 2020.

681

682 Deschamps-Berger, C., Cluzet, B., Dumont, M., Lafaysse, M., Berthier, E., Fanise, P., and Gascoin, S.:  
683 Improving the Spatial Distribution of Snow Cover Simulations by Assimilation of Satellite Stereoscopic  
684 Imagery, *Water Resour. Res.*, 58, e2021WR030271, <https://doi.org/10.1029/2021WR030271>, 2022.

685

686 Del Barrio, G., Creus, J., and Puigdefabregas, J.: Thermal Seasonality of the High Mountain Belts of the  
687 Pyrenees, *Mt. Res. Dev.*, 10, 227–233, 1990.

688 Devers, A., Vidal, J. P., Lauvernet, C., and Vannier, O.: FYRE Climate: A high-resolution reanalysis of daily  
689 precipitation and temperature in France from 1871 to 2012, *Climate of the Past*, 17, 1857–1879,  
690 <https://doi.org/10.5194/cp-17-1857-2021>, 2021.

691 Durand, Y., Giraud, G., Brun, E., Mérindol, L., and Martin, E.: A computer-based system simulating snowpack  
692 structures as a tool for regional avalanche forecasting, *Journal of Glaciology*, 45, 469–484,  
693 <https://doi.org/10.3189/s0022143000001337>, 1999.

694 Durand, Y., Laternser, M., Giraud, G., Etchevers, P., Lesaffre, B., and Mérindol, L.: Reanalysis of 44 yr of  
695 climate in the French Alps (1958–2002): Methodology, model validation, climatology, and trends for air  
696 temperature and precipitation, *J Appl Meteorol Climatol*, 48, 429–449,  
697 <https://doi.org/10.1175/2008JAMC1808.1>, 2009.

698 Essery, R.: A factorial snowpack model (FSM 1.0), *Geosci Model Dev*, 8, 3867–3876,  
699 <https://doi.org/10.5194/gmd-8-3867-2015>, 2015.

700

701 Essery, R., Kim, H., Wang, L., Bartlett, P., Boone, A., Brutel-Vuilmet, C., Burke, E., Cuntz, M., Decharme,  
702 B., Dutra, E., Fang, X., Gusev, Y., Hagemann, S., Haverd, V., Kontu, A., Krinner, G., Lafaysse, M., Lejeune,  
703 Y., Marke, T., Marks, D., Marty, C., Menard, C. B., Nasonova, O., Nitta, T., Pomeroy, J., Schädler, G.,  
704 Semenov, V., Smirnova, T., Swenson, S., Turkov, D., Wever, N., and Yuan, H.: Snow cover duration trends  
705 observed at sites and predicted by multiple models, *Cryosphere*, 14, 4687–4698, [https://doi.org/10.5194/tc-](https://doi.org/10.5194/tc-14-4687-2020)  
706 14-4687-2020, 2020.

707 Freudiger, D., Kohn, I., Stahl, K., and Weiler, M.: Large-scale analysis of changing frequencies of rain-on-  
708 snow events with flood-generation potential, *Hydrol Earth Syst Sci*, 18, 2695–2709,  
709 <https://doi.org/10.5194/hess-18-2695-2014>, 2014.

710 García-Ruiz, J. M., López-Moreno, J. I., Vicente-Serrano, S. M., Lasanta-Martínez, T. and Beguería, S.  
711 Mediterranean water resources in a global change scenario, *Earth Sci. Rev.*, 105(3–4), 121–139,  
712 <https://doi.org/10.1016/j.earscirev.2011.01.006>, 2011.

713 Garvelmann, J., Pohl, S., and Weiler, M.: Variability of observed energy fluxes during rain-on-snow and clear  
714 sky snowmelt in a midlatitude mountain environment, *J Hydrometeorol*, 15, 1220–1237,  
715 <https://doi.org/10.1175/JHM-D-13-0187.1>, 2014.

- 716 Günther, D., Marke, T., Essery, R., and Strasser, U.: Uncertainties in Snowpack Simulations—Assessing the  
 717 Impact of Model Structure, Parameter Choice, and Forcing Data Error on Point-Scale Energy Balance Snow  
 718 Model Performance, *Water Resour Res*, 55, 2779–2800, <https://doi.org/10.1029/2018WR023403>, 2019.
- 719 Habets, F., Boone, A., Champeaux, J. L., Etchevers, P., Franchistéguy, L., Leblois, E., Ledoux, E., le Moigne,  
 720 P., Martin, E., Morel, S., Noilhan, J., Seguí, P. Q., Rousset-Regimbeau, F., and Viennot, P.: The SAFRAN-  
 721 ISBA-MODCOU hydrometeorological model applied over France, *Journal of Geophysical Research*  
 722 *Atmospheres*, 113, <https://doi.org/10.1029/2007JD008548>, 2008.
- 723 Hansen, B.B., Isaksen, K., Benestad, R.E., et al.: Warmer and wetter winters: characteristics and implications  
 724 of an extreme weather event in the High Arctic. *Environ. Res. Lett.* 9, 114021.
- 725 Harder, P. and Pomeroy, J.: Hydrological model uncertainty due to precipitation-phase partitioning methods,  
 726 *Hydrological Processes*, 28, 4311–4327. <https://doi.org/10.1002/hyp.9799>, 2014.
- 727 Immerzeel, W. W., Lutz, A. F., Andrade, M., Bahl, A., Biemans, H., Bolch, T., Hyde, S., Brumby, S., Davies,  
 728 B. J., Elmore, A. C., Emmer, A., Feng, M., Fernández, A., Haritashya, U., Kargel, J. S., Koppes, M.,  
 729 Kraaijenbrink, P. D. A., Kulkarni, A. v., Mayewski, P. A., Nepal, S., Pacheco, P., Painter, T. H., Pellicciotti, F.,  
 730 Rajaram, H., Rupper, S., Sinisalo, A., Shrestha, A. B., Viviroli, D., Wada, Y., Xiao, C., Yao, T., and Baillie, J.  
 731 E. M.: Importance and vulnerability of the world’s water towers, *Nature*, 577, 364–369,  
 732 <https://doi.org/10.1038/s41586-019-1822-y>, 2020.
- 733 IPCC: High Mountain Areas, in: *The Ocean and Cryosphere in a Changing Climate*, Cambridge University  
 734 Press, 131–202, <https://doi.org/10.1017/9781009157964.004>, 2022.
- 735 Jennings, K. S., Winchell, T. S., Livneh, B., and Molotch, N. P.: Spatial variation of the rain-snow temperature  
 736 threshold across the Northern Hemisphere, *Nat Commun*, 9, <https://doi.org/10.1038/s41467-018-03629-7>,  
 737 2018.
- 738 il Jeong, D. and Sushama, L.: Rain-on-snow events over North America based on two Canadian regional  
 739 climate models, *Clim Dyn*, 50, 303–316, <https://doi.org/10.1007/s00382-017-3609-x>, 2018.
- 740 Kohler, J. and Aanes, R.: Effect of winter snow and ground-icing on a Svalbard reindeer population: Results  
 741 of a simple snowpack model, in: *Arctic, Antarctic, and Alpine Research*, 333–341,  
 742 [https://doi.org/10.1657/1523-0430\(2004\)036\[0333:EOWSAG\]2.0.CO;2](https://doi.org/10.1657/1523-0430(2004)036[0333:EOWSAG]2.0.CO;2), 2004.
- 743 Krinner, G., Derksen, C., Essery, R., Flanner, M., Hagemann, S., Clark, M., Hall, A., Rott, H., Brutel-  
 744 Vuilmet, C., Kim, H., Ménard, C. B., Mudryk, L., Thackeray, C., Wang, L., Arduini, G., Balsamo, G.,  
 745 Bartlett, P., Boike, J., Boone, A., Chéruf, F., Colin, J., Cuntz, M., Dai, Y., Decharme, B., Derry, J.,  
 746 Ducharne, A., Dutra, E., Fang, X., Fierz, C., Ghattas, J., Gusev, Y., Haverd, V., Kontu, A., Lafaysse, M.,  
 747 Law, R., Lawrence, D., Li, W., Marke, T., Marks, D., Ménégos, M., Nasonova, O., Nitta, T., Niwano, M.,  
 748 Pomeroy, J., Raleigh, M. S., Schaedler, G., Semenov, V., Smirnova, T. G., Stacke, T., Strasser, U.,  
 749 Svenson, S., Turkov, D., Wang, T., Wever, N., Yuan, H., Zhou, W., and Zhu, D.: ESM-SnowMIP: assessing  
 750 snow models and quantifying snow-related climate feedbacks, *Geosci. Model Dev.*, 11, 5027–5049,  
 751 <https://doi.org/10.5194/gmd-11-5027-2018>, 2018.
- 752 Lemus-Canovas, M., Lopez-Bustins, J. A., Trapero, L., and Martin-Vide, J.: Combining circulation weather  
 753 types and daily precipitation modelling to derive climatic precipitation regions in the Pyrenees, *Atmos Res*,  
 754 220, 181–193, <https://doi.org/10.1016/j.atmosres.2019.01.018>, 2019.
- 755 Lemus-Canovas, M., Lopez-Bustins, J. A., Martín-Vide, J., Halifa-Marin, A., Insua-Costa, D., Martinez-

- 756 Artigas, J., Trapero, L., Serrano-Notivol, R., and Cuadrat, J. M.: Characterisation of extreme precipitation  
757 events in the Pyrenees: From the local to the synoptic scale, *Atmosphere* (Basel), 12,  
758 <https://doi.org/10.3390/atmos12060665>, 2021.
- 759 Li, D., Lettenmaier, D. P., Margulis, S. A., and Andreadis, K.: The Role of Rain-on-Snow in Flooding Over  
760 the Conterminous United States, *Water Resour Res*, 55, 8492–8513, <https://doi.org/10.1029/2019WR024950>,  
761 2019.
- 762 Llasat, M. C., Marcos, R., Llasat-Botija, M., Gilabert, J., Turco, M., and Quintana-Seguí, P.: Flash flood  
763 evolution in North-Western Mediterranean, *Atmos Res*, 149, 230–243,  
764 <https://doi.org/10.1016/j.atmosres.2014.05.024>, 2014.
- 765 López-Moreno, J. I.: Recent variations of snowpack depth in the central Spanish Pyrenees, *Arct Antarct Alp*  
766 *Res*, 37, 253–260, [https://doi.org/10.1657/1523-0430\(2005\)037\[0253:RVOSDI\]2.0.CO;2](https://doi.org/10.1657/1523-0430(2005)037[0253:RVOSDI]2.0.CO;2), 2005.
- 767 López-Moreno, J.I., Goyette, S., and Beniston, M.: Climate change prediction over complex areas: spatial  
768 variability of uncertainties and predictions over the Pyrenees from a set of regional climate models.  
769 *International Journal of Climatology*, 28, 1535–1550. <https://doi.org/10.1002/joc.1645>, 2008.
- 770 López-Moreno, J. I., Pomeroy, J. W., Revuelto, J., and Vicente-Serrano, S. M.: Response of snow processes to  
771 climate change: Spatial variability in a small basin in the Spanish Pyrenees, *Hydrol Process*, 27, 2637–2650,  
772 <https://doi.org/10.1002/hyp.9408>, 2013.
- 773 López-Moreno, J. I., Pomeroy, J. W., Morán-Tejeda, E., Revuelto, J., Navarro-Serrano, F. M., Vidaller, I., and  
774 Alonso-González, E.: Changes in the frequency of global high mountain rain-on-snow events due to climate  
775 warming, *Environmental Research Letters*, 16, <https://doi.org/10.1088/1748-9326/ac0dde>, 2021.
- 776 López-Moreno, J.I., Soubeyroux, J.M., Gascoin, S., Alonso-González, E., Durán-Gómez, N., Lafaysse, M.,  
777 Vernay, M., Carmagnola, C. and Morin, S. Long-term trends (1958–2017) in snow cover duration and depth  
778 in the Pyrenees. *International Journal of Climatology*, 40, 1–15. <https://doi.org/10.1002/joc.6571>, 2020.
- 779 López-Moreno, J.I., and Vicente-Serrano, S.M.: Atmospheric circulation influence on the interannual  
780 variability of snowpack in the Spanish Pyrenees during the second half of the twentieth century, *Nord. Hydrol.*,  
781 38 (1), 38–44, <https://doi.org/10.2166/nh.2007.030>, 2007.
- 782 López-Moreno, J.I., and Latron, J., 2008. Spatial heterogeneity in snow water equivalent induced by forest  
783 canopy in a mixed beech-fir stand in the Pyrenees. *Ann. Glaciol.* 49 (1), 83–90,  
784 <https://doi.org/10.3189/172756408787814951>, 2008.
- 785 Loukas, A., Vasiliades, L., and Dalezios, N. R.: Potential climate change impacts on flood producing  
786 mechanisms in southern British Columbia, Canada using the CGCMA1 simulation results, *J. Hydrol.*, 259,  
787 163–188, [https://doi.org/10.1016/S0022-1694\(01\)00580-7](https://doi.org/10.1016/S0022-1694(01)00580-7), 2002
- 788 Lundquist, J. D., Dickerson-Lange, S. E., Lutz, J. A., and Cristea, N. C.: Lower forest density enhances snow  
789 retention in regions with warmer winters: A global framework developed from plot-scale observations and  
790 modeling, *Water Resour Res*, 49, 6356–6370, <https://doi.org/10.1002/wrcr.20504>, 2013.
- 791 Lynn, E., Cuthbertson, A., He, M., Vasquez, J. P., Anderson, M. L., Coombe, P., Abatzoglou, J. T., and Hatchett,  
792 B. J.: Technical note: Precipitation-phase partitioning at landscape scales to regional scales, *Hydrol Earth Syst*  
793 *Sci*, 24, 5317–5328, <https://doi.org/10.5194/hess-24-5317-2020>, 2020.
- 794 Matiu, M., Crespi, A., Bertoldi, G., Carmagnola, C.M., Marty, C., Morin, S., Schöner, W., Cat Berro, D.,

795 Chiogna, G., De Gregorio, L., Kotlarski, S., Majone, B., Resch, G., Terzago, S., Valt, M., Beozzo, W.,  
796 Cianfarra, P., Gouttevin, I., Marcolini, G., Notarnicola, C., Petitta, M., Scherrer, S.C., Strasser, U., Winkler,  
797 M., Zebisch, M., Cicogna, A., Cremonini, R., Debernardi, A., Faletto, M., Gaddo, M., Giovannini, L., Mercalli,  
798 L., Soubeyroux, J.-M., Susnik, A., Trenti, A., Urbani, S., Weilguni, V. Observed snow depth trends in the  
799 European Alps 1971 to 2019. *Cryosphere*, 1–50. <https://doi.org/10.5194/tc-2020-289>, 2020.

800 Marks, D., Link, T., Winstral, A., and Garen, D.: Simulating snowmelt processes during rain-on-snow over a  
801 semi-arid mountain basin, 1992.  
802

803 Martin, E., Brun, E., and Durand, Y.: Sensitivity of the French Alps snow cover to the variation of climatic  
804 variables, *Annales Geophysicae*, 12, 469–477, 1994.

805 Marty, C., Schlögl, S., Bavay, M., and Lehning, M.: How much can we save? Impact of different emission  
806 scenarios on future snow cover in the Alps, *Cryosphere*, 11, 517–529, <https://doi.org/10.5194/tc-11-517-2017>,  
807 2017.

808 Mazurkiewicz, A. B., Callery, D. G., and McDonnell, J. J.: Assessing the controls of the snow energy balance  
809 and water available for runoff in a rain-on-snow environment, *J Hydrol (Amst)*, 354, 1–14,  
810 <https://doi.org/10.1016/j.jhydrol.2007.12.027>, 2008.

811 Mazzotti, G., Essery, R., Webster, C., Malle, J., and Jonas, T.: Process-Level Evaluation of a Hyper-Resolution  
812 Forest Snow Model Using Distributed Multisensor Observations, *Water Resour Res*, 56,  
813 <https://doi.org/10.1029/2020WR027572>, 2020.

814 McCabe, G. J., Clark, M. P., and Hay, L. E.: Rain-on-snow events in the Western United-States,  
815 <https://doi.org/10.1175/BAMS-88-3-319>, 2007.

816 Mooney, P. A. and Li, L.: Near future changes to rain-on-snow events in Norway, *Environmental Research*  
817 *Letters*, 16, <https://doi.org/10.1088/1748-9326/abfdeb>, 2021.

818 Morán-Tejeda, E., López-Moreno, J. I., Stoffel, M., and Beniston, M.: Rain-on-snow events in Switzerland:  
819 Recent observations and projections for the 21st century, *Clim Res*, 71, 111–125,  
820 <https://doi.org/10.3354/cr01435>, 2016.

821 Morán-Tejeda, E., Fassnacht, S. R., Lorenzo-Lacruz, J., López-Moreno, J. I., García, C., Alonso-González, E.,  
822 and Collados-Lara, A. J.: Hydro-meteorological characterization of major floods in Spanish mountain rivers,  
823 *Water (Switzerland)*, 11, <https://doi.org/10.3390/W11122641>, 2019.

824 Morin, S., Horton, S., Techel, F., Bavay, M., Coléou, C., Fierz, C., Gobiet, A., Hagenmuller, P., Lafaysse, M.,  
825 Ližar, M., Mitterer, C., Monti, F., Müller, K., Olefs, M., Snook, J. S., van Herwijnen, A., and Vionnet, V.:  
826 Application of physical snowpack models in support of operational avalanche hazard forecasting: A status  
827 report on current implementations and prospects for the future,  
828 <https://doi.org/10.1016/j.coldregions.2019.102910>, 2020.

829 Musselman, K. N., Clark, M. P., Liu, C., Ikeda, K., and Rasmussen, R.: Slower snowmelt in a warmer world,  
830 *Nat Clim Chang*, 7, 214–219, <https://doi.org/10.1038/nclimate3225>, 2017a.

831 Musselman, K. N., Keitholotch, N. P., Mar, N., and Mgulis, S. A.: Snowmelt response to simulated warming  
832 across a large elevation gradient, southern sierra Nevada, California, *Cryosphere*, 11, 2847–2866,  
833 <https://doi.org/10.5194/tc-11-2847-2017>, 2017b.

- 834 Musselman, K. N., Lehner, F., Ikeda, K., Clark, M. P., Prein, A. F., Liu, C., Barlage, M., and Rasmussen, R.:  
 835 Projected increases and shifts in rain-on-snow flood risk over western North America,  
 836 <https://doi.org/10.1038/s41558-018-0236-4>, 2018.
- 837 Navarro-Serrano, F. and López-Moreno, J. I.: Análisis espacio-temporal de los eventos de nevadas en el pirineo  
 838 Español y su relación con la circulación atmosférica, Cuadernos de Investigacion Geografica, 43, 233–254,  
 839 <https://doi.org/10.18172/cig.3042>, 2017.
- 840 Ohba, M. and Kawase, H.: Rain-on-Snow events in Japan as projected by a large ensemble of regional climate  
 841 simulations, *Clim Dyn*, 55, 2785–2800, <https://doi.org/10.1007/s00382-020-05419-8>, 2020.  
 842
- 843 OPCC-CTP. Climate change in the Pyrenees: Impacts, vulnerabilities and adaptation bases of knowledge for  
 844 the future climate change adaptation strategy in the Pyrenees. 2018. 147. Jaca, Spain.  
 845 <https://www.opccctp.org/sites/default/files/editor/opcc-informe-en-paginas.pdf>. (last acces December 25,  
 846 2022)
- 847 Pall, P., Tallaksen, L. M., and Stordal, F.: A Climatology of Rain-on-Snow Events for Norway,  
 848 <https://doi.org/10.1175/JCLI-D-18>, 2019.
- 849 Pepin, N. C., Arnone, E., Gobiet, A., Haslinger, K., Kotlarski, S., Notarnicola, C., Palazzi, E., Seibert, P.,  
 850 Serafin, S., Schöner, W., Terzago, S., Thornton, J. M., Vuille, M., and Adler, C.: Climate Changes and Their  
 851 Elevational Patterns in the Mountains of the World, <https://doi.org/10.1029/2020RG000730>, 2022.
- 852 Peña-Angulo, D., Vicente-Serrano, S., Domínguez-Castro, F., Murphy, C., Reig, F., Tramblay, Y., Trigo, R.,  
 853 Luna, M.Y., Turco, M., Noguera, I., Aznarez-Balta, M., Garcia-Herrera, R., Tomas-Burguera, M. and Kenawy,  
 854 A. Long-term precipitation in Southwestern Europe reveals no clear trend attributable to anthropogenic  
 855 forcing. *Environmental Research Letters*, 15, 094070 <https://doi.org/10.1088/1748-9326/ab9c4f>, 2020.
- 856 Pons, M., López-Moreno, J., Rosas-Casals, M., and Jover, E.: The vulnerability of Pyrenean ski resorts to  
 857 climate-induced changes in the snowpack, *Clim. Change*, 131, 591–605, [https://doi.org/10.1007/s10584-015-](https://doi.org/10.1007/s10584-015-1400-8)  
 858 [1400-8](https://doi.org/10.1007/s10584-015-1400-8), 2015.
- 859 Pomeroy, J. W., Fang, X., and Rasouli, K.: Sensitivity of snow processes to warming in the Canadian Rockies,  
 860 2015.
- 861 Pomeroy, J. W., Fang, X., and Marks, D. G.: The cold rain-on-snow event of June 2013 in the Canadian Rockies  
 862 — characteristics and diagnosis, *Hydrol Process*, 30, 2899–2914, <https://doi.org/10.1002/hyp.10905>, 2016.
- 863 Rasouli, K., Pomeroy, J. W., and Whitfield, P. H.: Hydrological responses of headwater basins to monthly  
 864 perturbed climate in the North American Cordillera, *J Hydrometeorol*, 20, 863–882,  
 865 <https://doi.org/10.1175/JHM-D-18-0166.1>, 2019.
- 866 Rennert, K. J., Roe, G., Putkonen, J., and Bitz, C. M.: Soil thermal and ecological impacts of rain on snow  
 867 events in the circumpolar arctic, *J Clim*, 22, 2302–2315, <https://doi.org/10.1175/2008JCLI2117.1>, 2009.
- 868 Réveillet, M., Dumont, M., Gascoin, S., Lafaysse, M., Nabat, P., Ribes, A., Nheili, R., Tuzet, F., Ménégoz, M.,  
 869 Morin, S., Picard, G., and Ginoux, P.: Black carbon and dust alter the response of mountain snow cover under  
 870 climate change, *Nat Commun*, 13, <https://doi.org/10.1038/s41467-022-32501-y>, 2022.
- 871 Revuelto, J., Lecourt, G., Lafaysse, M., Zin, I., Charrois, L., Vionnet, V., Dumont, M., Rabatel, A., Six, D.,  
 872 Condom, T., Morin, S., Viani, A., and Sirguey, P.: Multi-criteria evaluation of snowpack simulations in

873 complex alpine terrain using satellite and in situ observations, *Remote Sens (Basel)*, 10,  
874 <https://doi.org/10.3390/rs10081171>, 2018.

875 Roe, G. H. and Baker, M. B.: Microphysical and Geometrical Controls on the Pattern of Orographic  
876 Precipitation, 2006.

877 Sanmiguel-Vallelado, A., McPhee, J., Esmeralda Ojeda Carreño, P., Morán-Tejeda, E., Julio Camarero, J., and  
878 López-Moreno, J. I.: Sensitivity of forest–snow interactions to climate forcing: Local variability in a Pyrenean  
879 valley, *J Hydrol (Amst)*, 605, <https://doi.org/10.1016/j.jhydrol.2021.127311>, 2022.

880

881 Schirmer, M., Winstral, A., Jonas, T., Burlando, P., and Peleg, N.: Natural climate variability is an important  
882 aspect of future projections of snow water resources and rain-on-snow events, *Cryosphere*, 16, 3469–3488,  
883 <https://doi.org/10.5194/tc-16-3469-2022>, 2022.

884 Schöner, W., Koch, R., Matulla, C., Marty, C., and Tilg, A. M.: Spatio-temporal patterns of snow depth within  
885 the Swiss-Austrian Alps for the past half century (1961 to 2012) and linkages to climate change, *International*  
886 *Journal of Climatology*, 39, 1589–1603, <https://doi.org/10.1002/joc.5902>, 2019.

887 Serrano-Notivoli, R., Buisan, S.T., Abad-Pérez, L.M., Sierra-Álvarez, E., Rodríguez-Ballesteros, C., López-  
888 Moreno, J.I. and Cuadrat, J.M. Tendencias recientes en precipitación, temperatura y nieve de alta montaña en  
889 los Pirineos (Refugio de Góriz, Huesca). In: *El clima: aire, agua, tierra y fuego*. Madrid, Spain: Asociación  
890 Española de Climatología y Ministerio para la Transición Ecológica – Agencia Estatal de Meteorología, pp.  
891 267, 1060–280, 2018.

892 Serrano-Notivoli, R., Mora, D., Ollero, A., Sánchez-Fabre, M., Sanz, P., and Saz, M.: Floodplain occupation  
893 and flooding in the central Pyrenees, *Cuadernos de Investigacion Geografica*, 43, 309–328,  
894 <https://doi.org/10.18172/cig.3057>, 2017.

895 Serreze, M. C., Gustafson, J., Barrett, A. P., Druckenmiller, M. L., Fox, S., Voveris, J., Stroeve, J., Sheffield,  
896 B., Forbes, B. C., Rasmus, S., Laptander, R., Brook, M., Brubaker, M., Temte, J., McCrystall, M. R., and  
897 Bartsch, A.: Arctic rain on snow events: Bridging observations to understand environmental and livelihood  
898 impacts, *Environmental Research Letters*, 16, <https://doi.org/10.1088/1748-9326/ac269b>, 2021.

899 Shanley, J. B. and Chalmers, A.: The effect of frozen soil on snowmelt runoff at Sleepers River, Vermont 1999.

900 Singh, P., Spitzbart, G., Hübl, H., and Weinmeister, H. W.: Hydrological response of snowpack under rain-on-  
901 snow events: a field study, *Journal of Hydrology*, 1–20 pp., 1997.

902 Smyth, E. J., Raleigh, M. S., and Small, E. E. (2020). Improving SWE estimation with data assimilation: The  
903 influence of snow depth observation timing and uncertainty. *Water Resources Research*, 56, e2019WR026853.  
904 <https://doi.org/10.1029/2019WR026853>

905 Spandre, P., François, H., Verfaillie, D., Lafaysse, M., Déqué, M., Eckert, N., George, E., and Morin, S.:  
906 Climate controls on snow reliability in French Alps ski resorts, *Sci Rep*, 9, <https://doi.org/10.1038/s41598-019-44068-8>, 2019.

907

908 Stewart, I. T.: Changes in snowpack and snowmelt runoff for key mountain regions,  
909 <https://doi.org/10.1002/hyp.7128>, 2009.

910 Surfleet, C. G. and Tullos, D.: Variability in effect of climate change on rain-on-snow peak flow events in a  
911 temperate climate, *J Hydrol (Amst)*, 479, 24–34, <https://doi.org/10.1016/j.jhydrol.2012.11.021>, 2013.

912 Szczypka, C., Gascoin, S., Houet, T., Hagolle, O., Dejoux, J.-F., Vigneau, C., and Fanise, P.: Impact of climate  
 913 and land cover changes on snow cover in a small Pyrenean catchment, *J. Hydrol.*, 521, 84–99,  
 914 doi:10.1016/j.jhydrol.2014.11.060, 2015.

915 Verfaillie, D., Lafaysse, M., Déqué, M., Eckert, N., Lejeune, Y., and Morin, S.: Multi-component ensembles  
 916 of future meteorological and natural snow conditions for 1500 m altitude in the Chartreuse mountain range,  
 917 *Northern French Alps, Cryosphere*, 12, 1249–1271, <https://doi.org/10.5194/tc-12-1249-2018>, 2018.

918 Vernay, M., Lafaysse, M., Monteiro, D., Hagenmuller, P., Nheili, R., Samacoïts, R., Verfaillie, D., and Morin,  
 919 S.: The S2M meteorological and snow cover reanalysis over the French mountainous areas: description and  
 920 evaluation (1958-2021), *Earth Syst Sci Data*, 14, 1707–1733, <https://doi.org/10.5194/essd-14-1707-2022>,  
 921 2022.

922 Vicente-Serrano, S.M., Rodríguez-Camino, E., Domínguez-Castro, F., El Kenawy, A., Azorín-Molina, C. An  
 923 updated review on recent trends in observational surface atmospheric variables and their extremes over Spain.  
 924 *Cuadernos de Investigación Geográfica (Geographical Research Letters)* 43 (1), 209-232.  
 925 <https://doi.org/10.18172/cig.3134>, 2017.

926 Vidaller, I., Revuelto, J., Izagirre, E., Rojas-Heredia, F., Alonso-González, E., Gascoin, S., René, P., Berthier,  
 927 E., Rico, I., Moreno, A., Serrano, E., Serreta, A., López-Moreno, J.I. Toward an ice-free mountain range:  
 928 Demise of Pyrenean glaciers during 2011–2020. *J. Geophys. Res. Lett.* 48, e2021GL094339  
 929 <https://doi.org/10.1029/2021GL094339>, 2021.

930 Viviroli, D., Archer, D. R., Buytaert, W., Fowler, H. J., Greenwood, G. B., Hamlet, A. F., Huang, Y.,  
 931 Koboltschnig, G., Litaor, M. I., López-Moreno, J. I., Lorentz, S., Schädler, B., Schreier, H., Schwaiger, K.,  
 932 Vuille, M., and Woods, R.: Climate change and mountain water resources: Overview and recommendations  
 933 for research, management and policy, *Hydrol Earth Syst Sci*, 15, 471–504, [https://doi.org/10.5194/hess-15-](https://doi.org/10.5194/hess-15-471-2011)  
 934 471-2011, 2011.

935 Westermann, S., Boike, J., Langer, M., Schuler, T. V., and Etzelmüller, B.: Modeling the impact of wintertime  
 936 rain events on the thermal regime of permafrost, *Cryosphere*, 5, 945–959, [https://doi.org/10.5194/tc-5-945-](https://doi.org/10.5194/tc-5-945-2011)  
 937 2011, 2011.

938 Wipf, S. and Rixen, C.: A review of snow manipulation experiments in Arctic and alpine tundra ecosystems,  
 939 <https://doi.org/10.1111/j.1751-8369.2010.00153.x>, 2010.

940 Wu, X., Che, T., Li, X., Wang, N., and Yang, X.: Slower Snowmelt in Spring Along With Climate Warming  
 941 Across the Northern Hemisphere, *Geophys Res Lett*, 45, 12,331-12,339,  
 942 <https://doi.org/10.1029/2018GL079511>, 2018.

943 Würzer, S., Jonas, T., Wever, N., and Lehning, M.: Influence of initial snowpack properties on runoff formation  
 944 during rain-on-snow events, *J Hydrometeorol*, 17, 1801–1815, <https://doi.org/10.1175/JHM-D-15-0181.1>,  
 945 2016.

946